Scalable TCR synthesis and screening enable antigen reactivity mapping in vitiligo

Article

Immunity

Scalable TCR synthesis and screening enable antigen reactivity mapping in vitiligo

Graphical abstract

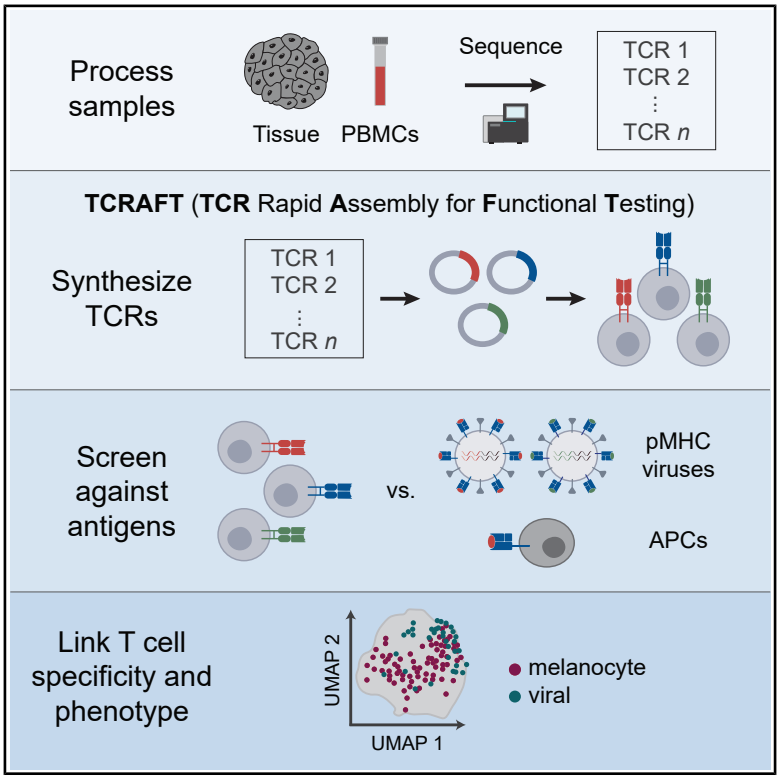

Authors

Stephanie A. Gaglione, Rachit S. Mukkamala, Chirag Krishna, ..., John E. Harris, Aaron Winkler, Michael E. Birnbaum

Correspondence

mbirnb@mit.edu

In brief

Mapping TCRs to antigens at scale presents a major challenge. Gaglione et al. develop an approach to rapidly synthesize and screen thousands of TCRs, enabling broad TCR-antigen screening. Examining T cell specificity in vitiligo uncovers autoreactive T cells with transcriptional programs similar to melanoma-reactive T cells, revealing shared features of disease-relevant T cells in autoimmunity and cancer.

Highlights

- TCRAFT enables rapid pooled synthesis of large TCR libraries
- TCRAFT integrates with RAPTR to screen the antigen specificity of TCRs in vitiligo
- TCR-antigen mapping uncovers transcriptional programs of autoreactive T cells

Gaglione et al., 2026, Immunity *59*, 1–17
February 10, 2026
https://doi.org/10.1016/j.immuni.2026.01.001

CellPress

Immunity

CellPress
OPEN ACCESS

Article

Scalable TCR synthesis and screening enable antigen reactivity mapping in vitiligo

Stephanie A. Gaglione,[1,2] Rachit S. Mukkamala,[2,3] Chirag Krishna,[4] Blake E. Smith,[2,5] Marc H. Wadsworth II,[4] Scott A. Jelinsky,[4] Caleb R. Perez,[2,3] Laura Schmidt-Hong,[5,6] Erica L. Katz,[7] Kyle J. Gellatly,[8] Lestat R. Ali,[9,10] Jiao Shen,[5,10] Patrick V. Holec,[11] Qingyang Henry Zhao,[2,3] Amanda O. Chan,[2,3] Ellen J.K. Xu,[2,3] Kellie M. Kravarik,[4] Julia A. Guzova,[4] Connor S. Dobson,[2,3] Harshabad Singh,[12,13] Manuel Garber,[8] Michael Dougan,[9,13] Stephanie K. Dougan,[5,10] John E. Harris,[7] Aaron Winkler,[4] and Michael E. Birnbaum[2,3,6,14,*]

[1]Department of Chemical Engineering, Massachusetts Institute of Technology, Cambridge, MA, USA
[2]Koch Institute for Integrative Cancer Research, Cambridge, MA, USA
[3]Department of Biological Engineering, Massachusetts Institute of Technology, Cambridge, MA, USA
[4]Inflammation & Immunology Research Unit, Pfizer Inc., Cambridge, MA 02139, USA
[5]Department of Immunology, Harvard Medical School, Boston, MA, USA
[6]Ragon Institute of MGH, MIT, and Harvard, Cambridge, MA, USA
[7]Department of Dermatology, University of Massachusetts Chan Medical School, 364 Plantation St, Worcester, MA, USA
[8]Program in Bioinformatics and Integrative Biology, University of Massachusetts Chan Medical School, Worcester, MA, USA
[9]Department of Medicine, Division of Gastroenterology, Massachusetts General Hospital and Harvard Medical School, Boston, MA, USA
[10]Department of Cancer Immunology and Virology, Dana-Farber Cancer Institute, Boston, MA, USA
[11]Fletcher Biosciences, Inc., Cambridge, MA, USA
[12]Department of Medical Oncology, Dana-Farber Cancer Institute, Boston, MA, USA
[13]Department of Medicine, Harvard Medical School, Boston, MA, USA
[14]Lead contact
*Correspondence: mbirnb@mit.edu
https://doi.org/10.1016/j.immuni.2026.01.001

SUMMARY

T cells initiate targeted immune responses using T cell receptors (TCRs) to recognize specific antigens. Mapping TCRs to antigens at scale remains a major challenge. Here, we developed an approach to synthesize and functionally screen tens of thousands of TCRs simultaneously. TCR rapid assembly for functional testing (TCRAFT) uses a modular strategy to rapidly and inexpensively construct large pools of TCRs from sequences while maintaining TCRα/β pairing. We applied TCRAFT to reconstruct over 3,800 TCRs from vitiligo blister fluid and mapped these TCRs to specific peptide-major histocompatibility complexes using RAPTR, an activation-based library-on-library screening approach. Vitiligo antigen-specific T cells displayed pronounced clonal expansion and transcriptomic signatures similar to antigen-specific T cells in melanoma, pointing to shared features of disease-relevant T cells in autoimmunity and cancer. Demonstrating scalability, we synthesized and screened over 30,800 TCRs from donors with pancreatic ductal adenocarcinoma to capture antigen-reactive TCRs. Our approach expands the scale and accessibility of TCR-antigen screening, which is critical to understanding immunity and developing new immunotherapies.

INTRODUCTION

T cells are central to adaptive immunity, responding to specific antigens in the context of cancer, infection, and autoimmunity via T cell receptors (TCRs). Each T cell clone expresses a unique TCR, a heterodimer composed of a TCRα and TCRβ chain, that binds to short peptides presented by major histocompatibility complex (MHC) proteins (pMHCs) to elicit an antigen-specific T cell response. Screening TCRs for antigen reactivity at a high throughput would advance our understanding of natural immune function while providing sources of therapeutically relevant TCRs and data for improving computational models of TCR specificity.[1,2] However, the vast diversity of the TCR repertoire—up to 10^8 unique clonotypes per individual[3,4]—makes large-scale mapping of TCR-antigen interactions a major challenge.

Identifying antigen-specific TCRs and their associated cell phenotypes is a critical priority in cancer[5] and autoimmune research.[6] T cells recognizing cancer-specific neoantigens often exhibit exhausted phenotypes,[7,8] and their role in tumor control is well documented.[9,10] By contrast, the phenotypic states and antigenic targets of T cells driving autoimmunity are less well understood. Proposed sources of autoantigens include self-antigens,[11] post-translationally modified epitopes,[12] and viral epitopes.[13] Vitiligo is one of the few autoimmune diseases with known antigens, largely due to insights from melanoma studies.

Please cite this article in press as: Gaglione et al., Scalable TCR synthesis and screening enable antigen reactivity mapping in vitiligo, Immunity (2026), https://doi.org/10.1016/j.immuni.2026.01.001

In both diseases, autoreactive CD8$^+$ T cells target melanocyte-derived antigens, including melanoma antigen recognized by T cells 1 (MART-1), tyrosinase, and gp100.[7,14–17] However, the extent of overlap in transcriptional features of antigen-specific T cells between vitiligo and melanoma remains unclear. Defining shared and distinct attributes of these T cell populations is essential for advancing targeted therapies in both cancer[5] and autoimmunity.[6]

Despite advances in single-cell and computational methods for sequencing and pairing TCR chains,[18,19] TCR datasets alone provide little insight into antigen specificity. Current screening strategies evaluate only a small subset of TCRs, typically selected based on clonotypic expansion or phenotypic markers.[1] Furthermore, assembling and screening TCR libraries remains costly, labor-intensive, and inefficient. Existing approaches rely on synthesizing expensive gene fragments, assembling individual TCRs in an array using custom oligonucleotides and libraries of TCR variable regions,[20–26] or amplifying TCRs from primary cell samples.[27–29] A key limitation of synthetic TCR assembly is maintaining the natural pairing between TCRα and TCRβ chains, which is essential for native TCR specificity. Current pooled TCR assembly methods either require co-transduction of separate TCR chains, an approach limited in scale, or scramble TCRα/β pairings, resulting in libraries dominated by non-functional TCRs.[30] While recent methods enable pooled assembly of up to 1,000 TCRs, error rates and technical complexity limit broad adoption or further increases in throughput.[31]

To address these limitations, we developed TCR rapid assembly for functional testing (TCRAFT), a scalable and cost-effective approach to easily synthesize tens of thousands of TCRs in a pool for under $1 per TCR. TCRAFT links pools of TCR variable region genes with CDR3α/β-containing oligonucleotides via three Golden Gate assembly steps, yielding paired-chain TCR libraries with >99% correctly assembled TCRs. We integrate TCRAFT with receptor-antigen pairing by targeted retroviruses (RAPTR),[32] a high-throughput antigen discovery platform, to enable one-pot library-versus-library screening of TCR reactivity. Using this system, we screened 3,808 TCR clonotypes from vitiligo lesions against 101 vitiligo- and melanoma-associated antigens, extracting precise TCR-antigen pairings in a single step. We orthogonally validated these hits and expanded reactivity screening to 561 antigens using an antigen presentation assay. By linking TCR specificity to corresponding gene expression data, we identified correlations between transcriptomic signatures of vitiligo- and melanoma-associated antigen-reactive T cells. To further demonstrate scalability, we used TCRAFT to synthesize a single library of 30,810 TCRs from surgically resected tumors and peripheral blood mononuclear cells (PBMCs) of patients with pancreatic ductal adenocarcinoma (PDAC) and identified antigen-specific TCRs using antigen-presenting cells pulsed with peptides.

By significantly reducing cost, labor, and technical barriers, TCRAFT provides an accessible and efficient strategy for assembling large TCR libraries. We couple these libraries with high-throughput antigen screening and single-cell transcriptomics to link TCR specificity to cell phenotype. Applied to vitiligo, this integrated approach uncovers transcriptional programs of melanocyte-reactive T cells. Together, these tools will accelerate efforts to decode TCR specificity, understand immune responses, and develop TCR-based immunotherapies.

RESULTS

Modular assembly of pooled TCR libraries by hierarchical Golden Gate assembly

Single-cell and repertoire TCR sequencing enable deep profiling of clonal T cell dynamics in autoimmune diseases such as vitiligo, but TCR sequences provide limited disease context without antigen specificity. To address this, we aimed to establish a complete TCR-antigen discovery pipeline consisting of single-cell sequencing to extract paired TCR chain sequences, pooled synthetic TCR assembly, and high-throughput library-on-library TCR-antigen screening (Figure 1A). We first sought to address the bottleneck of assembling large TCR libraries from sequencing data.

To enable low-cost pooled assembly of TCRs from sequences, we generate TCRαβ libraries using vector pools encoding germline alpha- and beta-chain variable (TRAV and TRBV) and constant (TRAC and TRBC) genes, as well as oligonucleotide pools of linked CDR3α/β sequences (Figure S1). We first insert the CDR3α/β-containing oligos into vectors with matching TRBV-TRAC sequences, followed by insertion of TRBC-P2A-TRAV sequences between the CDR3α and CDR3β sequences. The resulting product is a complete, synthetically formatted TCR (TRBV-TRBC-P2A-TRAV-TRAC), which is then transferred to an expression vector of choice via a third reaction (Figure 1B).

Our approach uses Golden Gate assembly to pair CDR3α/β fragments with TRAV and TRBV genes in a pooled setting (Figure 1C). This approach employs type IIS enzymes to generate four-base-pair overhangs, ensuring seamless linkage of coding regions. Although Golden Gate assembly has previously been demonstrated for assembling individual TCRs,[22] extending this approach to pooled library assembly remained infeasible due to the low orthogonality between four-base overhangs. To address this challenge, we leveraged a comprehensive 4-bp ligation fidelity dataset[33] to design highly orthogonal pairs of overhangs for each vector in the pool (Figure S1). Each TRBV-TRAC and TRBC-TRAV fragment was assigned a distinct, fixed pair of 5′ and 3′ overhangs to facilitate precise assembly with CDR3α/β-containing oligos while preserving coding sequences (Table S1). Oligos thus encode CDR3α, CDR3β, and a few amino acids from associated TRBV, TRAV, TRAC, and TRBC regions, each of which contains a specific fixed 4-bp overhang. While other pooled approaches employ long orthogonal sequences to link each CDR3α and CDR3β, causing assembly complexity to scale with the number of TCRs,[31] TCRAFT overcomes this limitation by encoding CDR3α and CDR3β on the same oligo and using fixed germline-defined overhangs. TCRAFT assembly complexity therefore remains constant regardless of the number of TCRs. Library size is determined by limits in oligo synthesis, the efficiency of bacterial electroporation to generate the plasmid library, and the sensitivity of downstream screening approaches. This design additionally allows for a fully standardized protocol for all reactions. We benchmark TCRAFT against other approaches and detail costs in Table S1. Collectively, TCRAFT is designed to rapidly assemble large TCR libraries in 6 days via three Golden Gate reactions using standard reagents, without liquid handling automation.

Please cite this article in press as: Gaglione et al., Scalable TCR synthesis and screening enable antigen reactivity mapping in vitiligo, Immunity (2026), https://doi.org/10.1016/j.immuni.2026.01.001

CellPress
OPEN ACCESS

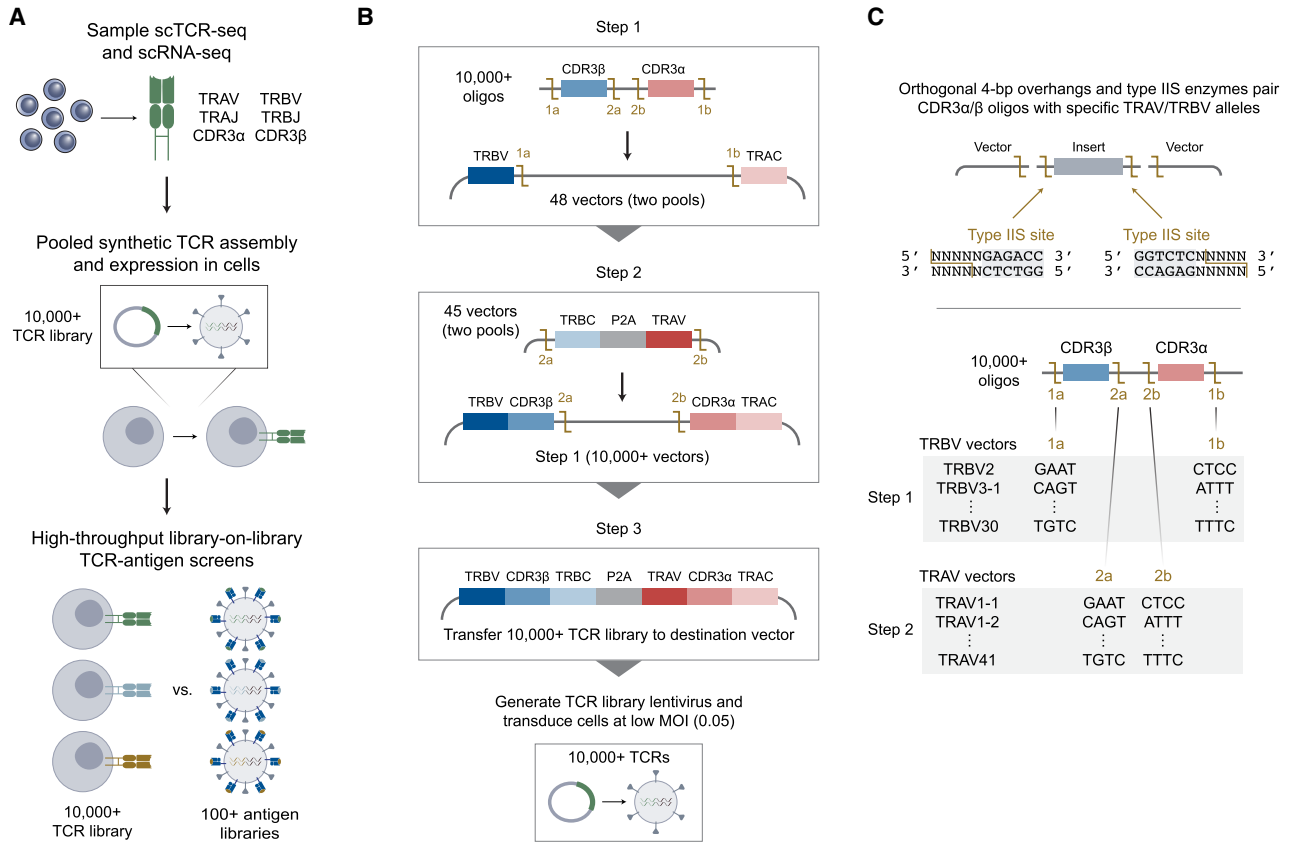

Figure 1. Overview of modular TCR assembly and screening pipeline

(A) Schematic of a high-throughput screening pipeline to identify antigen-specific TCRs by sequencing samples to extract paired TCRαβ receptor sequences (step 1), assembling a TCR library in a pool and expressing TCRs in cells (step 2), and pairing TCRs to cognate antigens in a library-on-library screen with lentiviruses pseudotyped with pMHCs or other antigen discovery methods (step 3).

(B) Schematic of pooled TCR assembly method. Step 1 inserts oligos of paired CDR3β-α sequences into TRBV-TRAC vectors to generate TRBV-CDR3β-CDR3α-TRAC. Step 2 inserts TRBC-P2A-TRAV fragments between CDR3β and CDR3α to generate complete TCRs. Step 3 transfers the complete TCRs to an expression vector. TCR libraries are expressed in cells via lentiviral transduction at a low MOI. All steps are completed via Golden Gate assembly.

(C) Schematic of approach to correctly pair TCR components. Type IIS enzymes generate 4-bp overhangs to facilitate ligation between reaction components. Each TRBV- and TRAV-containing vector contains unique pairs of 4-bp overhangs designed to maximize correct pairing while preserving coding sequences. Each CDR3α/β oligo contains four enzyme restriction sites, with the outer 4-bp overhangs facilitating pairing to TRBV vectors and inner 4-bp overhangs corresponding to TRAV vectors.

See also Figure S1.

Pooled assembly and characterization of a synthetic vitiligo 3,808 TCR library

To examine TCR reactivity in the context of vitiligo, we identified 3,808 TCRs in suction blister fluid from vitiligo lesions of 10 HLA-A*02:01^{+} (henceforth HLA-A2) donors (Figure 2A; Table S2). While prior work suggests that vitiligo is driven by CD8^{+} T cells reactive to MART-1 and other melanocyte-specific antigens,[34–37] perilesional T cell reactivity has not been broadly examined due to limitations in screening T cells from tissue samples. Vitiligo offers a compelling context for studying antigen-specific T cell responses in autoimmunity given its strong HLA-A2 risk association[37,38] and limited characterization of cellular mechanisms underlying a loss of tolerance.

We assembled these 3,808 vitiligo-associated TCRs using TCRAFT with greater than 1,000-fold coverage at each step. We analyzed the assembled TCR library via Oxford Nanopore long-read sequencing to evaluate correct pairing between TCR components and assess the TCR frequency distribution. Sequencing revealed highly accurate pairing between CDR3α and CDR3β sequences and their corresponding TRAV and TRBV alleles (Figures 2B, S2, and S3). 99.1% of sequences in the final product consist of correctly paired TRBV, TRAV, CDR3α, and CDR3β sequences corresponding to the 3,808 TCR list obtained from single-cell TCR sequencing (scTCR-seq) (Figure 2B). We detected 3,759 of 3,808 TCRs (98.7%) via long-read sequencing with a ~42-fold variation in TCR frequency between the 5th and 95th percentiles (Figures 2C and 2D). We complemented this analysis with short-read sequencing of both the TRAV-CDR3α and TRBV-CDR3β regions at greater sequencing depth and detected 99.9% of both CDR3α and CDR3β sequences (3,804/3,808).

Please cite this article in press as: Gaglione et al., Scalable TCR synthesis and screening enable antigen reactivity mapping in vitiligo, Immunity (2026), https://doi.org/10.1016/j.immuni.2026.01.001

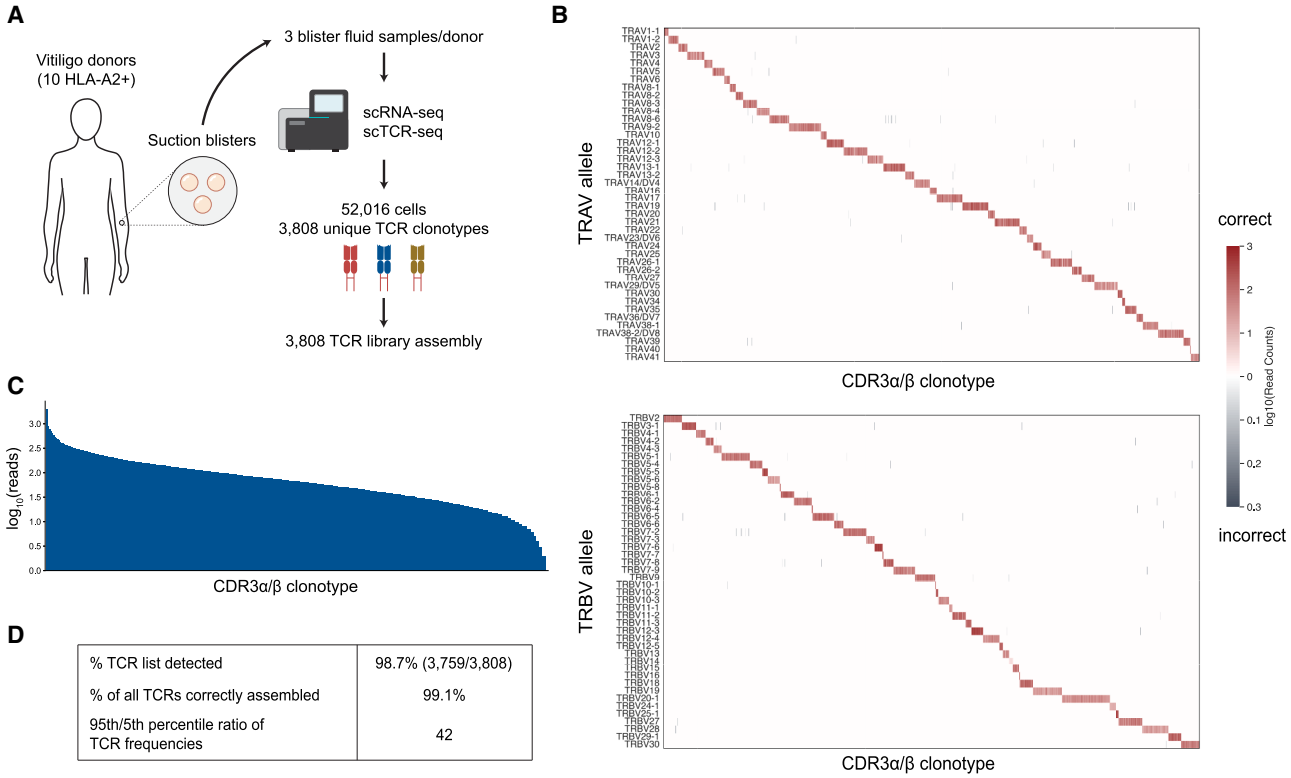

Figure 2. Pooled assembly of 3,808 TCRs from scTCR-seq of vitiligo blister fluid

(A) Sample origin and extraction of 3,808 TCRαβ clonotypes. Blister fluid samples from 10 HLA-A2$^+$ vitiligo donors were analyzed via 10× scRNA-seq, scTCR-seq, and CITE-seq to capture 3,808 unique TCR clonotypes with matched gene expression data.

(B) Heatmap depicting accuracy of TRAV and TRBV allele pairing to CDR3α and CDR3β sequences, respectively, as $\log_{10}$-transformed read counts of all TRAV-CDR3α and TRBV-CDR3β combinations. Red indicates correct pairing, and gray indicates incorrect pairing.

(C) Log_{10}-transformed read counts of complete, correctly assembled TCRs.

(D) Summary data on the proportion of 3,808 TCRs detected, the proportion of all TCRs correctly assembled, and frequency distribution.

See also Figures S2 and S3 and Table S1.

Library-on-library TCR-antigen screen using pMHC-pseudotyped lentiviruses

To screen these TCRs for reactivity, we expressed our 3,808 vitiligo-associated TCR library in a clonal TCR-null Jurkat J76 T cell line encoding an NFAT-CFP reporter.[39] Most approaches to screen TCRs against antigens for reactivity are limited to individual antigens or fail to generate data on interacting TCR-antigen pairs. Barcoded pMHC tetramers can be used to map TCRs to antigens[40,41] but are logistically complex to scale to many antigens and are limited by variable pMHC folding and multimerization, barcode cross-contamination, noise from aggregation, and saturated signal from high-affinity interactions.[1] We and others have demonstrated the feasibility of using pMHC-displaying lentiviruses to infect antigen-specific TCR-expressing cells and extract paired TCR-antigen information with single-cell sequencing via the approaches RAPTR, ENTER-seq, and V-CARMA.[32,42,43] While in principle allowing for high-throughput antigen screening, our original RAPTR platform relied upon pMHC tetramers to pre-enrich TCRs from large libraries. Noting that pMHC-pseudotyped lentiviruses potently activate TCR-expressing cells, we optimized RAPTR to extract paired TCR-antigen data for 3,808 TCRs against 101 HLA-A2-binding antigens in one step using a highly sensitive NFAT reporter[39] (Figure 3A). By capturing cells both activated and transduced by pMHC viruses, we can minimize noise from non-specific transduction. This high selectivity is essential for screening large TCR libraries and eliminates laborious pre-enrichment steps.

We constructed a list of 101 HLA-A2-binding epitopes composed of melanoma-associated antigens,[44] vitiligo-associated antigens in the Immune Epitope Database (IEDB),[45] and known viral antigens from cytomegalovirus (CMV), Epstein-Barr virus (EBV), human T-lymphotropic virus 1 (HTLV-1), yellow fever virus (YFV), influenza A virus (IAV), and SARS-CoV-2 (Table S2). We then assembled a RAPTR library, with each epitope represented by a pMHC-pseudotyped lentivirus containing a matched barcode to enable integration into bulk and single-cell sequencing workflows (Figure S4). Improving upon the prior RAPTR workflow, we used the 101-pMHC virus library to both activate and transduce antigen-specific cells. After stimulating the 3,808 TCR library with the 101-pMHC virus library, we sorted activated TCR-expressing cells expressing an NFAT reporter (CFP$^+$), a subset of which were transduced (GFP$^+$) (Figure 3B).

As a feature of our assembly method, we codon-optimized CDR3α/β oligos to be fully unique, allowing complete TCR identities to be determined by sequencing either CDR3α or CDR3β.

Please cite this article in press as: Gaglione et al., Scalable TCR synthesis and screening enable antigen reactivity mapping in vitiligo, Immunity (2026), https://doi.org/10.1016/j.immunu.2026.01.001

CellPress
OPEN ACCESS

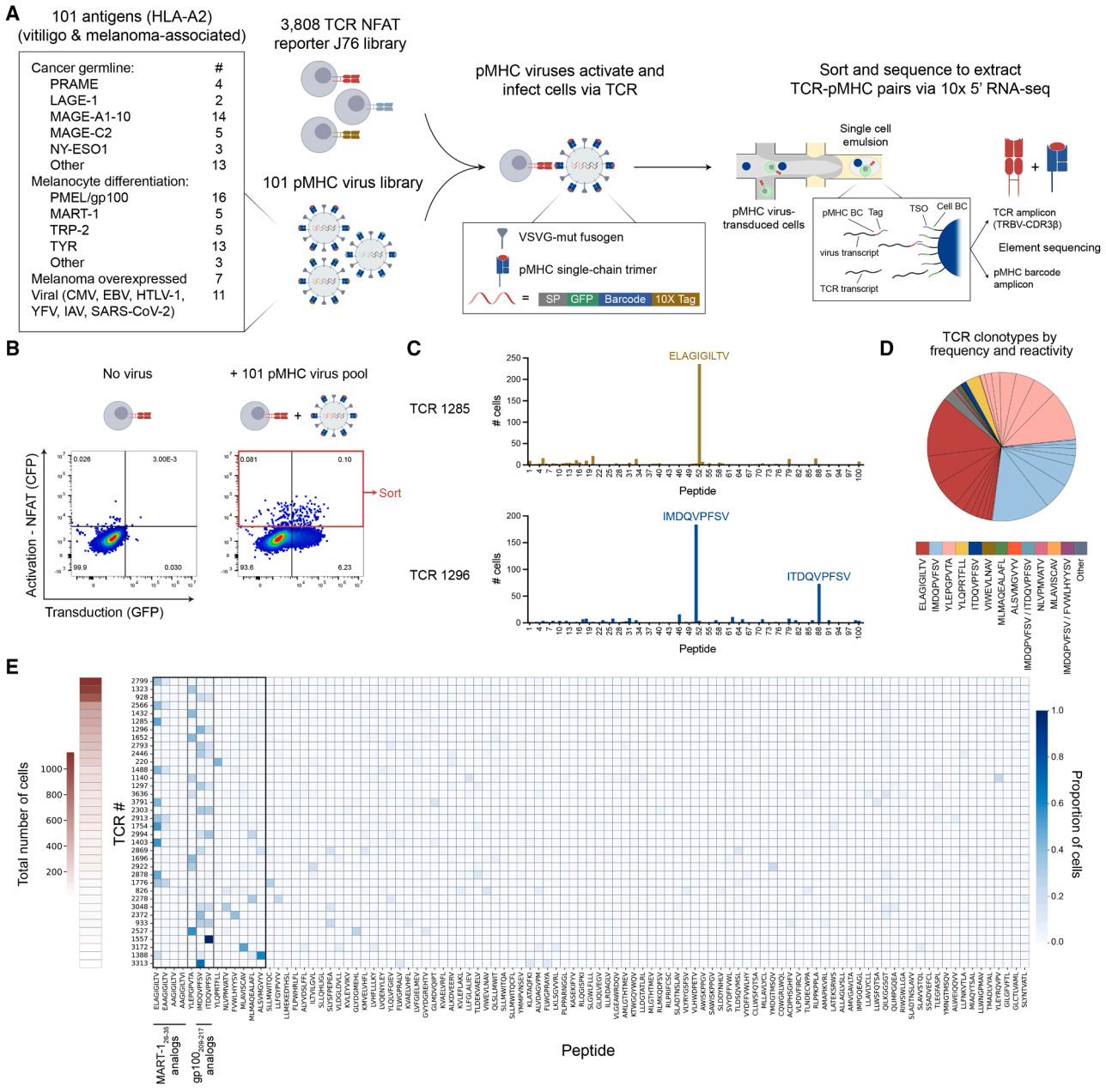

Figure 3. RAPTR enriches and pairs reactive TCRs with antigens

(A) Schematic of TCR library screen with 101 pMHC-pseudotyped lentiviruses to extract TCR-antigen pairs. 3,808 TCR-expressing NFAT reporter J76 cells are mixed with a 101-pMHC virus library containing vitiligo, melanoma, and viral antigens. Cells activated and transduced by the virus library are sorted and single-cell sequenced to capture reactive TCRs and cognate antigens.

(B) Cells activated (CFP^+) and transduced (GFP^+) by 101-pMHC virus library. Activated CFP^+ cells and CFP^+GFP^+ cells are sorted to capture both TCRs reactive to pMHC virus and virally integrated pMHC barcodes. CFP^+GFP^+ cells are sequenced via 10× single-cell sequencing.

(C) Bar plots for two enriched TCRs (TCR #1285 and #1296 as examples) showing the number of cells assigned each pMHC identity from single-cell sequencing. Each cell is assigned the pMHC identity with the highest UMI count. Each TCR clonotype is annotated as reactive to pMHCs with the most associated cells. TCR #1285 is reactive to ELAGIGILTV (MART-$1_{26–35}$), while TCR #1296 is reactive to IMDQVPFSV and ITDQVPFSV (gp$100_{209–217}$).

(D) Summary of reactive TCR clonotypes showing frequency (wedge size) and antigen reactivity (color) of each clonotype.

(E) Heatmap depicting the distribution of pMHC assignments for each reactive TCR clonotype, sorted by total TCR frequency (*y* axis). Each row represents a TCR clonotype, and values correspond to the sample data depicted in (C), scaled to the total number of cells. MART-$1_{26–35}$ and gp$100_{209–217}$ analogs, as well as other epitopes assigned to TCRs, are grouped and boxed on the left side of the heatmap.

See also Figures S4–S6 and Table S2.

Please cite this article in press as: Gaglione et al., Scalable TCR synthesis and screening enable antigen reactivity mapping in vitiligo, Immunity (2026), https://doi.org/10.1016/j.immuni.2026.01.001

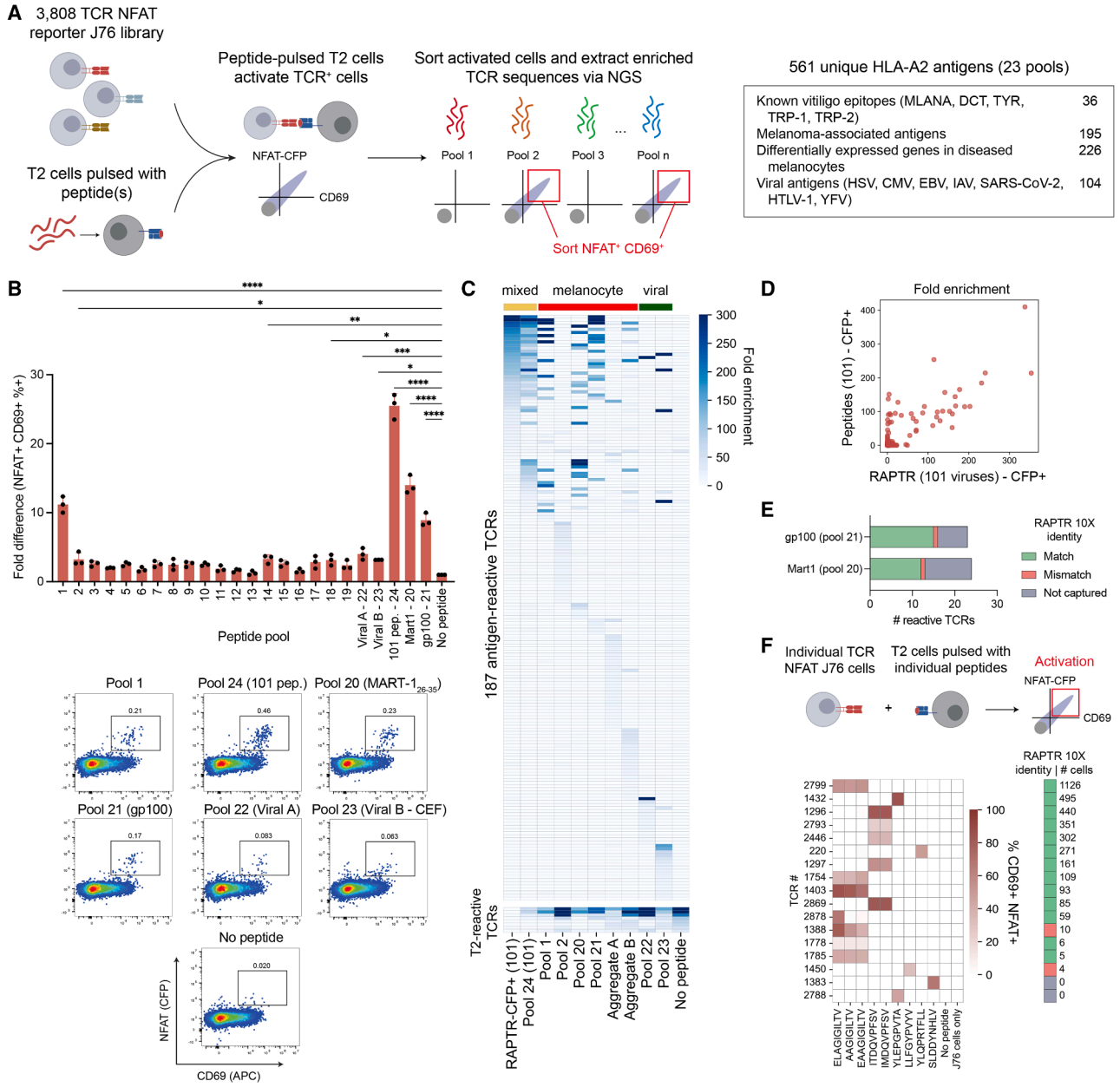

Figure 4. Expanded reactivity screen of 3,808 TCRs and validation with antigen presentation assay

(A) Schematic of screening approach. 3,808 TCR-expressing NFAT reporter J76 cells are cocultured with HLA-A2$^+$ T2 cells pulsed with 24 pools of peptides (561 unique antigens). Activated (NFAT-CFP$^+$) cells are sorted and sequenced via next-generation sequencing (NGS) to capture reactive TCRs.

(B) Bar plots and representative flow plots of cells activated by peptide pools. Bars report the ratio of % cells NFAT$^+$CD69$^+$ for peptide pools versus the no-peptide control. Data shown as mean ± SD for 3 replicates.

(C) Heatmap depicting TCRs >10-fold enriched by the 101 virus library (RAPTR), 101 peptide pool, or indicated peptide pools. Fold enrichment was calculated by dividing the frequency of each TCR in sorted cells with the starting frequency in the naive 3,808 TCR library. Several TCRs enriched in both the no peptide (T2 cells only) and peptide pool conditions, as shown in the second heatmap, and these TCRs are not considered to be antigen-reactive. RAPTR-CFP$^+$ represents NGS analysis of cells activated by 101-pMHC virus library (CFP$^+$). Aggregate A consists of pools stimulating a >1.5-fold increase in activation, and aggregate B consists of pools stimulating a 1- to 1.5-fold increase in activation.

(D) Plot depicting fold enrichment of all TCRs activated by pMHC viruses and peptides (CFP$^+$). Each dot represents a TCR clonotype.

(E) Bar plot showing TCRs reactive to pool 20 (MART-1$_{26–35}$ analogs) and pool 21 (gp100$_{280–288}$ and gp100$_{209–217}$ analogs) with associated RAPTR single-cell identity. RAPTR assigned a pMHC identity that matches (green) or mismatches (red) the peptide data. Gray indicates TCRs not captured by RAPTR.

(legend continued on next page)

Please cite this article in press as: Gaglione et al., Scalable TCR synthesis and screening enable antigen reactivity mapping in vitiligo, Immunity (2026), https://doi.org/10.1016/j.immuni.2026.01.001

To extract paired TCR-pMHC information, we performed single-cell RNA sequencing (scRNA-seq) on the transduced cell subset using 10× Genomics GEM-X 5′ chemistry. We included a targeted primer at the reverse transcription step and developed a custom amplification protocol to capture the TCRβ chain and identify complete TCR clonotypes. We additionally included a 10× Genomics capture tag sequence in the viral genome analogous to ENTER-seq.[42] This capture tag enables viral genomes, encoding pMHC barcodes, to be directly captured by the template switch oligo (TSO) on 10× 5′ gel bead-in emulsion (GEM) beads.

After filtering for doublets, we recovered 8,557 cells with paired TCR and pMHC information. Each cell was assigned a TCR and pMHC identity based on the ratio of unique molecular identifiers (UMIs) for the dominant TCR or pMHC relative to all TCR or pMHC UMIs for that cell. Each TCR identity was then paired to a cognate pMHC by examining the pMHC assignments of all corresponding cells expressing a given TCR. For example, TCR #1285 recognizes a MART-1_{26-35} analog, ELAGIGILTV, while TCR #1296 recognizes two $gp100_{209-217}$ analogs, IMDQVPFSV and ITDQVPFSV (Figure 3C). Collectively, a total of 54 candidate TCR clonotypes were captured with at least 5 total cells per clonotype, including 36 TCRs with at least 10 cells per clonotype, predominantly annotated as recognizing MART-1_{26-35} analogs, $gp100_{209-217}$ analogs, and $gp100_{280-288}$ (Figures 3D and 3E; Table S2). We observed a strong association between cells infected by viruses displaying MART-1_{26-35} analogs ELAGIGILTV and EAAGIGILTV, as well as $gp100_{209-217}$ analogs ITDQVPFSV and IMDQVPFSV. Recovering a high quantity of cells increases confidence in assigning a pMHC identity to a given clonotype, but TCR-antigen pairs can be unambiguously established with as few as 5 cells. Some low-frequency (<0.5%) clonotypes were assigned 2–3 possible pMHC identities (Figure 3D), indicating a potential limit of detection.

Detection and validation of antigen-reactive TCRs with peptide-pulsed APCs

We next screened the 3,808 vitiligo TCR J76 library against peptide-pulsed antigen-presenting cells (APCs) to validate putative antigen-reactive TCR clonotypes captured by our single-cell RAPTR workflow, demonstrate the compatibility of our TCR assembly strategy with a well-precedented and widely used antigen discovery method, and capture antigen-reactive TCRs against a broader array of pMHCs (Figure 4A). We generated a list of 561 antigens consisting of known vitiligo epitopes from the IEDB (36), an expanded list of melanoma-associated antigens (195),[44,46,47] 10 differentially expressed genes in diseased melanocytes filtered for binding to HLA-A2 using NetMHCpan4.1[48] (226), and viral antigens (104) (Table S2). The 101 antigens represented by the RAPTR pMHC virus library are a subset of this broader 561-antigen list. We assembled 23 pools encompassing 561 unique peptides, separated by melanocyte or viral origin, and a single pool of 101 peptides corresponding to the RAPTR virus library. Noting that RAPTR identified MART-1_{26-35}, $gp100_{280-288}$, and $gp100_{209-217}$ analogs as immunodominant epitopes, we created separate pools (20 and 21) for these peptides.

Upon stimulating the vitiligo TCR J76 library with TAP-deficient HLA-$A2^+$ T2 cells pulsed with pools encompassing 561 unique peptides, we observed TCR activation (NFAT$^+$ CD69$^+$) in response to several pools (Figure 4B). The 101-antigen pool elicited the most significant activation, consistent with its inclusion of known vitiligo epitopes, particularly MART-1_{26-35}, $gp100_{280-288}$, and $gp100_{209-217}$ analogs. Accordingly, vitiligo- and melanoma-associated peptide pools #1, 20, and 21 containing these analogs stimulated over five-fold greater activation than the negative control. Most melanocyte peptide pools induced only modest activation, though six pools were statistically significant. Both viral peptide pools also activated a significant proportion of cells.

To efficiently capture antigen-reactive TCRs, we sorted cells activated (NFAT-CFP$^+$ CD69$^+$) by peptide pools #1, 2, 20, 21, 22, 23, and 24 (101-peptide pool). Noting subtle activation by the other melanocyte peptide pools, we stimulated cells with these pools individually before aggregating cells into two groups prior to sorting. Aggregate group A consisted of pools that elicited a >1.5-fold increase in activation, while aggregate group B included pools that stimulated a 1- to 1.5-fold increase over the negative control (Table S2). We then PCR-amplified the TCRβ chain from genomic DNA to capture CDR3β sequences of enriched TCRs by next-generation sequencing (NGS).

We compared TCR frequencies in enriched cells against the naive 3,808 TCR J76 cell line to identify antigen-reactive TCRs. Across all activation stimuli, including 24 peptide pools and the 101-virus RAPTR library, 187 unique TCR clonotypes enriched more than 10-fold compared with the naive library after filtering TCRs also enriched by the no-peptide control (Figure 4C; Table S2). Given that peptide pools were split by melanocyte or viral origin, we classified TCRs as melanocyte-reactive if activated by pools #1 to 21 and viral-reactive if reactive to pools #22 and 23. 138 TCR clonotypes were unambiguously reactive to melanocyte antigens, while 38 clonotypes reacted to viral antigens. Of the 138 melanocyte-reactive clonotypes, 24 TCRs recognized MART-1_{26-35} (EAAGIGILTV) and associated analogs, while 23 TCRs recognized $gp100_{280-288}$ (YLEPGPVTA) and $gp100_{209-217}$ analogs (ITDQVPFSV and IMDQVPFSV). We excluded four clonotypes (TCR #726, 2413, 1588, and 3443) activated by both viral and melanocyte peptide pools, but not by the no-peptide control. TCRs enriched regardless of their initial frequency in the naive 3,808 TCR library, with no bias toward TCRs at a higher initial abundance (Figure S5). Both peptide-pulsed APCs and pMHC-displaying viruses activated and enriched TCRs from starting frequencies as low as 0.0003%, with seven clonotypes enriching from <0.001% of the naive library. We additionally noted several TCR clonotypes enriched by all peptide pools and the no-peptide control. These TCRs

(F) Heatmap showing activation (% NFAT-CFP$^+$CD69$^+$) of individual TCR-expressing NFAT reporter J76 cells with individual peptide-pulsed T2 cells for TCR clonotypes identified via RAPTR or peptide pool screens. TCR-antigen pairs are classified as matched (green), mismatched (red), or not captured (gray) by the RAPTR single-cell workflow, with the number of cells per clonotype indicated. p values are calculated with a one-way ANOVA (unpaired) with Dunnett's correction for multiple comparisons. $^{****}p < 0.0001$, $^{***}p < 0.001$, $^{**}p < 0.01$, $^{*}p < 0.05$; n.s., $p \geq 0.05$.
See also Figures S4–S6 and Table S2.

Please cite this article in press as: Gaglione et al., Scalable TCR synthesis and screening enable antigen reactivity mapping in vitiligo, Immunity (2026), https://doi.org/10.1016/j.immuni.2026.01.001

are reactive to T2 cells but not the RAPTR pMHC virus library, highlighting a potential strength of pMHC-pseudotyped lentiviruses.

Noting that the RAPTR pMHC viral library is a potent antigen-specific activator of T cells, we additionally set out to compare TCRs activated by our 101-member RAPTR viral library against a matched peptide pool. We sorted and bulk sequenced all T cells activated (CFP^+) or activated and transduced (CFP^+GFP^+) by the 101-pMHC virus library, as well as cells activated (CFP^+) by the 101-peptide pool (Figure S6). The top 27 reactive TCR clonotypes are the same for all conditions (Figures S6A and S6B), with similar clonotype enrichment by both peptides and viruses (Figure 4D). TCR clonotypes activated by pMHC viruses (CFP^+) are also transduced (CFP^+GFP^+) (Figures S6A and S6E). Comparing TCRs enriched by peptides and pMHC viruses beyond the top 27 clonotypes, we observe that each stimulus excludes several TCRs, 15 for viruses and 22 for peptides (Figure S6B), partly attributable to the definition of reactive as >10-fold enriched from the naive TCR library. The strong concordance between TCR clonotypes enriched by peptides and pMHC viruses affirms our ability to extract reactive TCR clonotypes with orthogonal antigen discovery methods.

The reactive TCRs include 33 of 36 TCR clonotypes with >10 cells in the RAPTR single-cell analysis, with the three missing clonotypes representing only 0.32% of enriched cells. To validate hits, we examined clonotypes enriched by MART-$1_{26–35}$ analogs (pool 20), as well as $gp100_{280–288}$ and $gp100_{209–217}$ analogs (pool 21) (Figure 4E). TCR-antigen pairs captured via RAPTR largely correspond, with one mismatched clonotype per pool. These mismatched TCRs are low frequency in the single-cell data, with 6 cells for TCR #1388 (pool 20) and 26 cells for TCR #3048 (pool 21). Most TCRs not captured by RAPTR single-cell analysis (gray) also failed to enrich >10-fold for the 101-peptide pool or viruses. Given that the concentration of individual peptides in pools 20 and 21 is ~10-fold higher than in the 101-peptide pool, we hypothesize that these TCRs may be less sensitive to antigen stimulation.

As further validation, we established individual clonal TCR J76 cell lines for a selection of TCRs and verified reactivity to individually peptide-pulsed T2 cells (Figure 4F). Of these, 13 TCR-antigen pairs identified via single-cell sequencing align with individual T2-peptide stimulation data, with two mismatched low-frequency clonotypes. By integrating large-scale TCR assembly and reactivity screening with pMHC-displaying viruses and peptide-pulsed APCs, we enable large-scale screening of thousands of TCRs from tissue-derived TCRs.

Phenotypes and antigen reactivity of blister fluid TCRs in vitiligo

We next sought to examine the gene expression programs of antigen-specific TCRs in vitiligo using our scRNA-seq dataset. Antigen-specific T cells have been reported to exhibit tissue-resident memory (T_{RM})[49] and cytotoxic phenotypes,[36] yet the functional interplay and contributions of these cell states to vitiligo pathogenesis remain unclear. Paradoxically, the same T cell phenotypes implicated in autoimmunity are broadly protective in melanoma and other cancers.[50,51] Although vitiligo and melanoma share antigenic targets,[7,14–17] it remains unclear whether antigen-specific T cells adopt similar transcriptional programs in the context of an inflammatory autoimmune setting versus the immunosuppressive tumor microenvironment. Although chronic antigen exposure occurs in both contexts, thus far it has not been possible to directly compare T cell transcriptional states of known antigen-reactive T cells in autoimmunity and cancer.

To address these questions, we created an atlas of T cell phenotypes for all 10 donors via unsupervised clustering (Figures 5A and S7; Table S3) paired with TCR-seq data evaluated for antigen reactivity. Most cells captured were $CD8^+$. A minority of cells were regulatory T cells, as evidenced by expression of *FOXP3* (Figure S7). Among $CD8^+$ T cells, we observed a "cytotoxic CD8" cluster defined by high expression of multiple granzymes and perforin (*PRF1*), consistent with prior literature highlighting the role of cytotoxic $CD8^+$ T cells in vitiligo.[52] This phenotype was corroborated by high expression of *HLA-DRB1* in this cluster (Figure S7). We further detected two clusters characterized by expression of *ZNF683 (HOBIT)*, a key transcription factor marking tissue-resident $CD8^+$ T cells, and the chemoattractant *GPR183 (EBI2)*, marking $CD8^+$ T cells in an activated and migratory state.[53]

To resolve the identities of these clusters and compare them to known T cell phenotypes in vitiligo, we surveyed expression of effector molecules, cytokines, chemokines, and transcription factors across the entire T cell atlas. The cytotoxic CD8 T cell cluster expressed high levels of multiple granzymes, including *GZMA*, *GZMB*, *GZMH*, and *GZMM*, but did not display high expression of *GZMK* (Figure S7), in contrast to the $CD8^+$ $GZMK^+$ cells previously shown to drive pathogenesis in rheumatoid arthritis[55] and airway inflammation.[56] Suggesting an exhausted state, the cytotoxic CD8 cluster expressed *PDCD1*, *CTLA4*, and *TIGIT* (Figure S7). Among cytokines and chemokines, *IFNG* and *CCL4/5* were predominantly expressed, in addition to *IL32* (Figures 5B and S7), which previous studies link to effector T cell responses in skin inflammation.[57–59] The tissue-resident cluster was broadly *HOBIT*$^+$ *CD69*$^+$ *ITGAE (CD103)*$^+$ *CD49A (ITGA1)*$^-$, consistent with prior reports.[60–62] Although *ITGAE (CD103)* was most highly expressed in our "tissue-resident" cluster (Figure S7; Table S3), both *CD69* and *ZNF683* were also detected at a lower level across the T cell atlas (Figure S7). This aligns with observations that $CD8^+$ T cells generally adopt a T_{RM} phenotype in vitiligo.[60–62]

To define the phenotypes of clonally expanded and antigen-reactive TCRs, we analyzed scTCR-seq and scRNA-seq data (Table S3). A total of 619 melanocyte-reactive T cells, representing 138 TCR clonotypes (Table S3), were distributed over multiple clusters in the T cell atlas, with the majority localized to the $CD8^+$ cytotoxic cluster (Figure 5B). We further examined TCRs reactive to MART-1_{26-35}, hereafter MART-1 (Figure 5C; N = 24 TCRs, 147 cells), a key antigen in both vitiligo[49] and melanoma.[63] These T cells were highly enriched in the $CD8^+$ cytotoxic cluster and demonstrated strong transcriptional upregulation of TRAV12-2 relative to other melanocyte-reactive TCRs (Figure S7B; Table S3). Viral-reactive clones were broadly distributed across similar transcriptional clusters as the melanocyte-reactive clones but were relatively underpowered in our dataset (Figure 5D; N = 38 TCRs, 84 cells). By contrast, cells harboring TCRs that were highly clonally expanded but not captured as reactive ("top undetected

Please cite this article in press as: Gaglione et al., Scalable TCR synthesis and screening enable antigen reactivity mapping in vitiligo, Immunity (2026), https://doi.org/10.1016/j.immuni.2026.01.001

CellPress
OPEN ACCESS

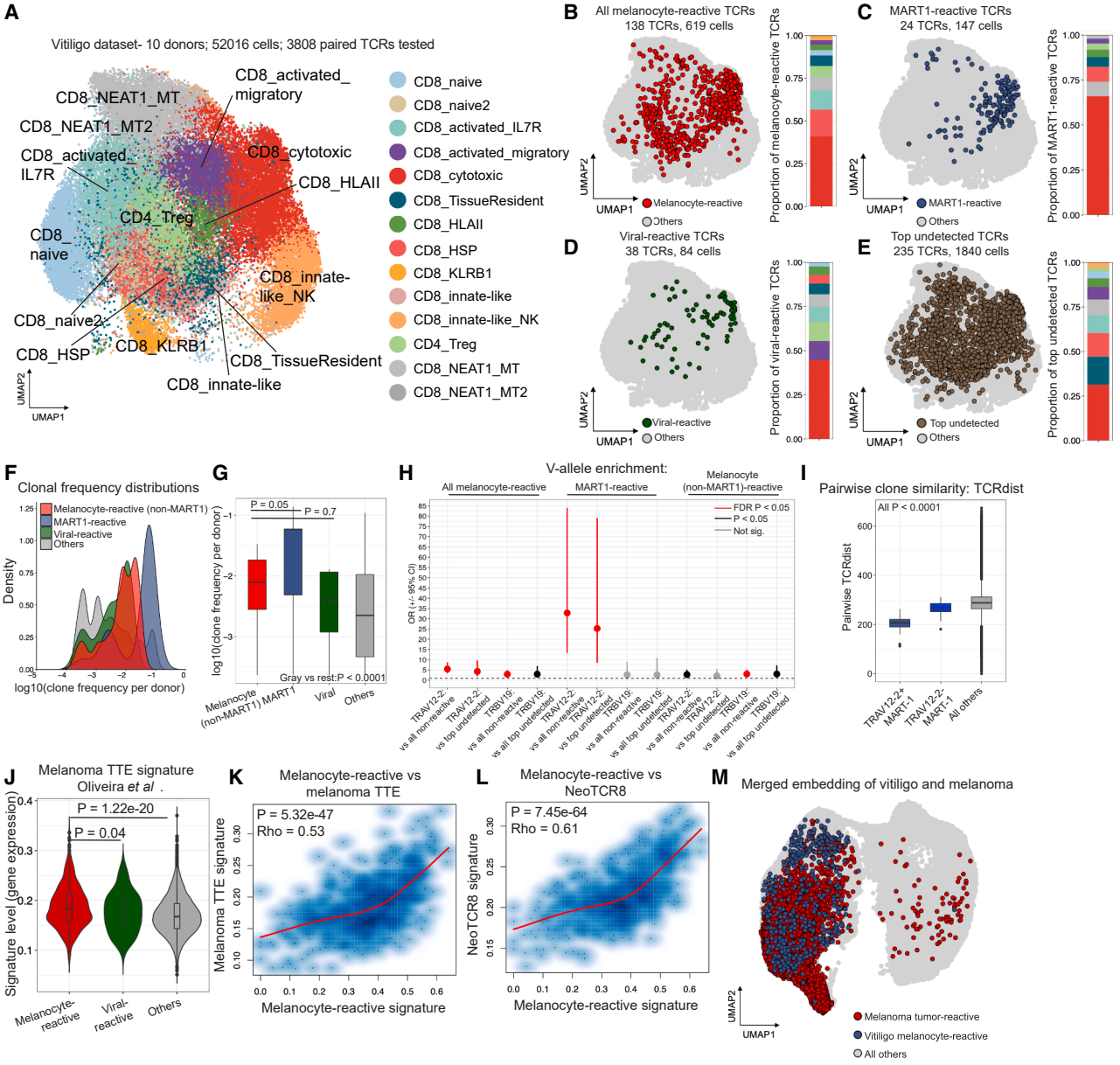

Figure 5. Phenotypes of TCRs with detected antigen reactivity

(A) UMAP representation of T cell clusters from integrated single-cell RNA sequencing (scRNA-seq) analysis of 10 vitiligo donors.

(B–E) Transcriptional cluster distribution of all melanocyte-reactive TCRs (B), MART1-reactive TCRs (C), viral-reactive TCRs (D), and top undetected TCRs (E).

(F and G) Clonal frequency distribution of antigen-detected TCR clonotypes versus non-antigen-detected TCR clonotypes ("others"). Clone frequency is calculated per donor. Data show antigen-detected clonotypes have a higher clonal frequency compared with non-antigen-detected clonotypes.

(H) Enrichment of variable gene segments in antigen-detected TCR clonotypes compared with non-reactive clonotypes. Statistics were computed using Fisher's exact test.

(I) Pairwise clone similarity computed using TCRdist between pairs of clonotypes in the indicated groups.

(J) Application of the TTE gene signature from Oliveira et al.[7] to clonotypes in our dataset.

(K) Correlation of melanocyte-reactive gene expression signature with the melanoma TTE signature across all cells with antigen-reactive TCRs.

(L) Correlation of the NeoTCR8 gene signature from Lowery et al.[54] across all cells in (K).

(M) Merged embedding of scRNA-seq data from vitiligo blister fluid (our data) and melanoma tissue data from Oliveira et al.[7]

p values are calculated using two-sided Wilcoxon tests for pairwise comparisons between antigen-reactive groups and Spearman correlation for correlation analyses. See also Figures S7–S10 and Table S3.

Please cite this article in press as: Gaglione et al., Scalable TCR synthesis and screening enable antigen reactivity mapping in vitiligo, Immunity (2026), https://doi.org/10.1016/j.immuni.2026.01.001

TCRs") demonstrated a moderately decreased enrichment in the CD8$^+$ cytotoxic cluster (Figure 5E). Differential expression analysis comparing the transcriptional phenotypes of top undetected TCRs to those of melanocyte-reactive TCRs revealed widespread differential expression of TCR variable gene segments (Figure S7B; Table S3), suggesting that altered antigen and/or HLA specificity, rather than altered T cell state, is the defining feature of the top undetected TCRs. Melanocyte-reactive TCRs exhibited higher clonal frequencies across and within individual donors compared with viral-reactive TCRs and non-antigen-detected TCRs ("others") (Figures 5F, 5G, and S7C). Moreover, MART-1-reactive TCRs are more clonally expanded relative to other melanocyte-reactive TCRs. These findings underscore the importance of MART-1 recognition in vitiligo pathogenesis and the capacity of our approach to detect TCRs specific for disease-associated antigens.

Previous studies have reported biased germline V allele usage in antigen-specific TCRs in autoimmunity.[64] To investigate whether antigen-specific TCRs are similarly restricted in vitiligo, we compared individual V or J allele usage in melanocyte-reactive clonotypes relative to other TCRs. Both TRAV12-2 and TRBV19 were significantly enriched in melanocyte-reactive TCRs relative to all non-reactive TCRs or top undetected clones, largely driven by MART-1 reactivity (Figure 5H; Table S3).

We next used TCRdist[65] to explore and quantify sequence similarities between antigen-reactive TCRs, focusing on MART-1-reactive clonotypes. TRAV-12$^+$ MART-1-reactive TCRs demonstrated high pairwise similarity relative to TRAV-12$^-$ MART-1-reactive, top undetected, and non-reactive TCRs (Figures 5I and S8A). This similarity is not observed if TCRdist is computed based on CDR3 sequences (Figure S8B), confirming that TRAV12-2 drives clustering of TRAV12-2$^+$ MART-1-reactive TCRs. We next examined pairwise TCR distance distributions to assess whether antigen-reactive clones were systematically missed. MART-1-reactive clonotypes enriched in the lowest decile of pairwise TCR distances ("G1"), with prevalence decreasing at greater distances (Figures S8C and S8D). Consistent with our clustering analysis, TRAV-12$^+$ MART-1-reactive TCRs dominate the lowest pairwise distances (Figures S8E and S8F). The lack of co-clustering between MART-1-reactive and non-reactive TCRs suggests that we largely captured MART-1-reactive clonotypes, while other melanocyte-reactive TCRs exhibit low clustering with diverse sequences.

The presence of effector and exhaustion markers on antigen-specific T cells in vitiligo prompted us to assess their transcriptional similarity to T cells in melanoma. We derived signatures of melanocyte-reactive and viral-reactive TCRs (Table S3) in vitiligo blister fluid and applied previously published gene expression signatures of antigen-specific CD8$^+$ T cells in melanoma[7] to our dataset (Figures 5J and S9A). Among melanoma tumor-specific T cell signatures derived in Oliveira et al.,[7] the terminal exhausted (TTE) signature was most strongly enriched in our vitiligo melanocyte-reactive T cells compared with non-reactive cells (Figures 5J and S9A). Genes shared between our melanocyte-reactive signature and the TTE signature included *CCL5*, *GZMB*, *HOPX*, *MTSS1*, and *PRF1*. A second, independent neoantigen-reactive T cell signature (NeoTCR8)[54] showed similar enrichment among our melanocyte-reactive T cells (Figures 5L, S9A, and S9C). Further, all tumor-specific signatures from Oliveira et al.[7] correlated with our derived melanocyte-reactive T cell signature, with the strongest correlations observed for the TTE and T progenitor exhausted (TPE) signatures (Figures 5K and S9B). We noted comparable enrichment and correlation with the NeoTCR8 signature (Figure S9A).

We next merged our vitiligo scRNA-seq data with melanoma scRNA-seq data from Oliveira et al.,[7] confirming that our melanocyte signature was enriched in tumor-reactive T cells (Figures S9D–S9F). Visualization of antigen-reactive clones from both vitiligo and melanoma on the merged embedding confirmed their overall transcriptional similarity (Figures 5M and S10). Nonetheless, differential gene expression analysis reveals subtle differences between the two cell states (Figure S10; Table S3), with HLA-II genes, antigen processing components (e.g., *CD74*), and *LAG3* upregulated in melanoma tumor-reactive T cells, whereas genes related to TCR signaling (e.g., *CD3G*, *CD48*, and *CD81*) and *IL7R* were upregulated in vitiligo-reactive cells. Collectively, these results suggest largely shared CD8$^+$ T cell transcriptional phenotypes between vitiligo and melanoma, although the tumor microenvironment imposes subtle changes in antigen-reactive T cells.

Assembly and antigen reactivity screening of a 30,000+ TCR library

With a validated methodology to construct TCR libraries, we next set out to determine if we could efficiently assemble tens of thousands of TCRs in a single reaction workflow. We compiled 30,810 TCR sequences derived from tumor-infiltrating lymphocytes (TILs) from surgically resected tumors and matched PBMCs from 21 donors with PDAC, as well as PBMCs from 9 PDAC and 2 healthy donors[66,67] (Figure 6A; Table S2). We ordered CDR3α/β oligos at a cost of $0.30 per TCR and assembled the TCR library using TCRAFT. Analogous to the 3,808 TCR library, we characterized the product with both Oxford Nanopore long-read sequencing and short-read Element sequencing. CDR3α and CDR3β sequences accurately paired with their corresponding TRAV and TRBV alleles, with 99.1% of assembled sequences forming correctly assembled TCRs and 99.6% (30,681/30,810) of TCRs detected via long-read sequencing (Figure 6B). TCR frequencies spanned ~36-fold between the 5th and 95th percentiles, a modest distribution suitable for a variety of screening methods (Figures 6C and 6D). Short-read sequencing captured 99.9% of CDR3α and CDR3β sequences (30,772/30,810).

To evaluate our ability to isolate rare antigen-reactive TCRs from this large TCR library, we expressed the 30,810 TCR library in a clonal NFAT-CFP reporter J76 T cell line. To experimentally validate that the library was functional, we activated the TCR library with T2 cells pulsed with the previously used pool of 96 seroprevalent viral (CEF) HLA-A2-binding epitopes and select individual peptides: influenza-derived GL9 (GILGFVFTL), CMV-derived NLV (NLVPMVATV), and EBV-derived GLC (GLCTLVAML), and sorted activated cells for TCR sequencing analysis. Five donors with available haplotypes were HLA-A*02:01$^+$, and the library incorporates TCRs from both TILs and PBMCs. We thus anticipated a small proportion of the TCRs to be potentially reactive to these immunodominant

Please cite this article in press as: Gaglione et al., Scalable TCR synthesis and screening enable antigen reactivity mapping in vitiligo, Immunity (2026), https://doi.org/10.1016/j.immuni.2026.01.001

CellPress
OPEN ACCESS

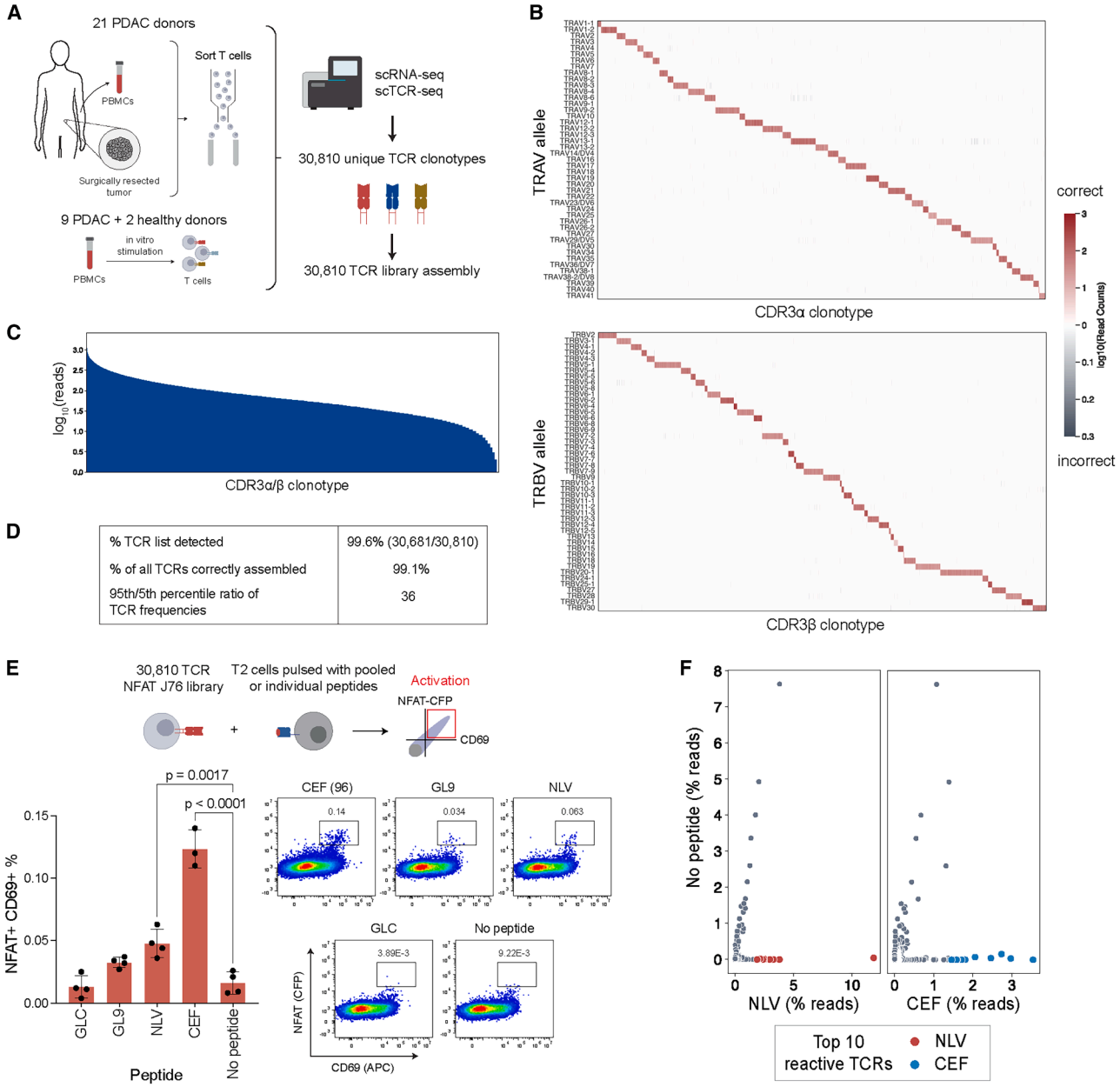

Figure 6. Pooled assembly of 30,810 TCRs from scTCR-seq of PDAC tumor resections and PBMCs

(A) Sample origin and extraction of 30,810 TCRαβ clonotypes.

(B) Heatmap depicting accuracy of TRAV and TRBV allele pairing to CDR3α and CDR3β sequences as $\log_{10}$-transformed read counts of all TRAV-CDR3α and TRBV-CDR3β combinations. Red and gray indicate correct and incorrect pairing, respectively.

(C) Log_{10}-transformed read counts of complete, correctly assembled TCRs.

(D) Summary data on the proportion of 30,810 TCRs detected, the proportion of all TCRs correctly assembled, and frequency distribution.

(E) Screen of 30,810 TCR library with peptide-pulsed T2 cells (individual peptides and a 96-member CEF peptide pool). Bar plot shows activation as a percentage of cells $\text{NFAT}^+\text{CD69}^+$ with representative flow plots for each antigen or pool. Data are represented as mean ± SD for $n = 4$ replicates. p values were calculated with a one-way ANOVA (unpaired) with Dunnett's correction for multiple comparisons.

(F) Scatterplot representing TCR clonotypes enriched by T2 cells pulsed with NLV, CEF pool, or no peptide (negative control). Enriched cells were processed via NGS to extract TCR clonotypes. TCR frequencies are depicted with each dot representing a unique TCR clonotype. Colored dots indicate the top 10 TCR clonotypes enriched exclusively by NLV peptide (red) or CEF (blue).

See also Figures S2, S3, S5, and S6 and Table S2.

Please cite this article in press as: Gaglione et al., Scalable TCR synthesis and screening enable antigen reactivity mapping in vitiligo, Immunity (2026), https://doi.org/10.1016/j.immuni.2026.01.001

epitopes. We captured reactivity to the CEF peptide pool ($p < 0.0001$) and NLV peptide ($p = 0.0017$) by a small fraction of cells (Figure 6E). We sorted cells reactive to T2 cells pulsed with the 96-peptide CEF pool, T2 cells pulsed with NLV peptide, and T2 cells without peptide as a negative control. We then sequenced CDR3β amplicons to identify activated TCRs for each condition and examined their frequency in the naive library (Figure S5E). Of the ten most abundant clonotypes enriched by NLV but not the no-peptide control (Figure 6F), seven contained α or β chains documented as NLV-specific in VDJDb.[68] Two of these clonotypes match TCRs known to recognize NLV (Table S2), and three clonotypes are from a donor confirmed to be HLA-A2$^+$.[65,69] The top 40 clonotypes enriched by NLV are listed in Table S2. Consistent with the presence of NLV in the 96-peptide pool, NLV-reactive TCRs represent a subset of those enriched by the CEF peptide pool (Figure S6F). To further validate these TCRs, we re-stimulated NLV-enriched cells with T2 cells pulsed with NLV peptide and no peptide. Sorting activated (NFAT-CFP$^+$CD69$^+$) cells, we recovered the same top NLV-reactive TCRs (Figure S6G). Our approach to assembling large synthetic TCR libraries enables the sensitive identification of low-frequency antigen-reactive TCRs.

DISCUSSION

Scalable, cost-effective synthesis and functional screening of TCR libraries with high accuracy are essential to decoding TCR-antigen specificity. We have integrated single-cell CD8$^+$ T cell profiling, pooled low-cost assembly of thousands of TCRs, and library-on-library TCR-antigen screening to build a broadly adoptable TCR-antigen screening pipeline and to examine transcriptomic signatures of antigen-reactive TCRs. Our TCR assembly approach, TCRAFT, enables low-cost, pooled synthesis of tens of thousands of TCRs with >99% assembly accuracy while maintaining native α/β pairing. Immortalized TCR-expressing cells facilitate deep profiling of irreplaceable samples, including blister fluid and resected tumor in this study, that would otherwise be infeasible to study with primary cell screens.[7,20–22,24,29,70] This approach additionally enables rounds of enrichment, repeated screens with different sets of antigens, functional characterization, and TCR-antigen pairing in a single step using RAPTR. By integrating TCRAFT with an optimized RAPTR pipeline, we achieved efficient, one-pot screening of TCR-antigen interactions, allowing identification of antigen-specific TCRs from thousands of TCRs with matched gene expression data. Using this pipeline, we screened 3,808 TCRs derived from vitiligo lesions of 10 donors against 101 antigens in a library-versus-library format and an expanded set of 561 antigens classified by melanocyte or viral origin. We further synthesized a 30,810-TCR library in a single reaction and demonstrated the compatibility of both TCR libraries with peptide-pulsed antigen-presenting cell screening. By linking antigen specificity to scRNA-seq data for vitiligo lesion-associated TCRs, we identified signatures of both melanocyte- and viral-reactive TCRs and shared transcriptional phenotypes with antigen-specific T cells in melanoma.

Advances in single-cell methods for sequencing paired TCR chains have produced large TCR datasets with little data on antigen specificity. Fewer than 1 million unique TCR-antigen pairs are known, with less than 4% of these TCRs including both TCR α and β chains.[2] Current pipelines for reconstructing and evaluating TCR sequences for specificity are largely confined to research groups with specialized expertise and typically focus on individual TCRs selected based on clonotypic expansion or phenotype. Although large-scale TCR synthesis and screening would provide unbiased antigen reactivity profiling, existing strategies are expensive, scale-limited, or difficult to execute, requiring liquid handling or specific optimization for each TCR library. By contrast, TCRAFT is affordable (<$1/TCR), freely available, easy to implement, and compatible with an array of antigen discovery methods. We anticipate that these features will enable broad use, leading to a significant increase in the number and diversity of known TCR-antigen pairs. This will accelerate the identification of clinically relevant TCRs for adoptive cell therapies and engineered therapeutics while providing valuable training data for computational models predicting TCR specificity.

Characterizing antigen-specific T cells in autoimmunity is crucial to decoding disease pathogenesis, developing diagnostic markers, and designing targeted immunotherapies. Analysis of paired scRNA-seq and TCR-seq data from vitiligo blister fluid revealed that melanocyte- and viral-reactive TCRs span multiple transcriptional states. Underscoring the specificity and sensitivity of our screening pipeline, TCRs identified as vitiligo antigen-specific exhibited pronounced clonal expansion. These T cells primarily adopted a cytotoxic phenotype characterized by expression of granzymes, *IFNG*, *CCL4/5*, *PRF1*, and exhaustion markers such as *PDCD1*. Gene signature analysis of antigen-reactive T cells in our dataset revealed significant correlation with antigen-specific T cells in melanoma, particularly with terminally exhausted CD8$^+$ T cells. The molecular mechanisms driving convergent phenotypes of T cell cytotoxicity and exhaustion in autoimmunity and cancer remain to be determined but are likely driven by chronic antigen exposure.[71,72] Our data suggest that T cell exhaustion is a common phenotype of antigen-specific T cells across autoimmunity and cancer. Notably, genetic analyses have associated vitiligo with reduced incidence of melanoma,[73] raising the possibility that antigen-reactive T cells in one setting may confer protection in another.

Paired with new methods to capture TCR sequences such as TIRTL-seq,[19] our approach for large-scale TCR assembly and screening using RAPTR and peptide-pulsed APCs completes a pipeline to generate TCR specificity data at an unprecedented scale. Given the extensive work expressing TCRs in both primary and Jurkat cells, we expect that our TCR library assembly approach will be compatible with any workflow utilizing TCR-expressing cells.[7,11,31,39,74–82] TCRAFT should also readily integrate with other antigen discovery approaches, including T-Scan,[11,79] MCR-TCRs,[80] TCR-MAP,[78] pMHC multimers,[40] and screening of minigene libraries,[81] expanding the scale of known TCR-antigen interactions. By enabling rapid and cost-effective TCR assembly and seamlessly integrating TCR libraries with multiple antigen screening methods, this pipeline has the potential to advance immunotherapy, accelerate vaccine design, and deepen our understanding of TCR recognition.

Please cite this article in press as: Gaglione et al., Scalable TCR synthesis and screening enable antigen reactivity mapping in vitiligo, Immunity (2026), https://doi.org/10.1016/j.immuni.2026.01.001

Limitations of the study

This integrated approach to synthesize, express, and deorphanize TCRs has several limitations. Although RAPTR is theoretically capable of screening thousands of antigens,[32] we limited our screen to 101 antigens due to the cost and logistical challenge of building large viral libraries. At present, RAPTR requires a one-time arrayed transfection step to generate a viral packaging cell line that can then be used to produce pooled viral libraries. Recent advances in constructing viral packaging cell lines in pool[83,84] and automation may significantly reduce this cost and increase the scale of RAPTR screens.

Even at the scale of thousands of antigens, RAPTR and most existing antigen discovery approaches require pre-selecting HLA alleles and potential antigens. Our study screened a total of 561 HLA-A*02:01-binding antigens and found only ~5% of the TCR repertoire to be reactive to these antigens. It is likely that other TCRs in the library are melanocyte-reactive, either to other antigens bound to HLA-A*02:01 or other MHCs, but were not detected in our screen. Improvements to screening approaches such as RAPTR, functional screening in primary cells, and the incorporation of peptide-MHC datasets from sources including immunopeptidomics, whole exome sequencing, and RNA sequencing will likely improve the antigen identification rate for orphan TCRs.

We applied TCRAFT, RAPTR, and an APC-based assay to screen TCR reactivity with Jurkat cells, an approach well-suited for profiling low-frequency TCRs and irreplaceable samples. Synthetic TCR libraries can also be expressed in primary cells for functional assays (i.e., AIM)[82] and to examine potential differences in antigen sensitivity between Jurkat and primary cells.[24] Further, although TCRAFT is currently designed for reconstructing human TCR repertoires, this design framework can be readily applied to develop equivalent systems for other organisms.

Despite these limitations, this work demonstrates cost-effective, large-scale TCR synthesis, functional screening, and TCR-antigen mapping from sequencing data, enabling deep profiling of scarce samples. These advances establish a broadly adoptable platform to link T cell specificity to transcriptomic state and build a foundation for expanded study of T cell recognition in diverse disease contexts.

RESOURCE AVAILABILITY

Lead contact

Further information and requests for resources and reagents should be directed to and will be fulfilled by the lead contact, Michael Birnbaum (mbirnb@mit.edu).

Materials availability

TCRAFT plasmids are available as a kit on Addgene (Birnbaum group), both pre-pooled (https://www.addgene.org/pooled-library/birnbaum-human-tcraft/, Cat #1000000264) and as individual plasmids (https://www.addgene.org/kits/birnbaum-tcraft/, Cat #1000000271). Additional plasmids are available upon request.

Data and code availability

Code to generate oligo pools for TCRAFT, analyze TCR library composition, and process NGS and single-cell RAPTR sequencing data is available on GitHub at https://github.com/birnbaumlab/TCRAFT/ and https://github.com/birnbaumlab/Gaglione-et-al-2025. NGS and RAPTR scRNA-seq datasets are available in the National Center for Biotechnology Information Sequence Read Archive under accession number PRJNA1247142. scRNA-seq and scTCR-seq data are available at https://singlecell.broadinstitute.org/single_cell/study/SCP3412/scalable-tcr-synthesis-and-screening-enables-antigen-reactivity-mapping-in-vitiligo (accession number SCP3412). Any additional information required to reanalyze the data reported in this paper is available from the lead contact upon request.

ACKNOWLEDGMENTS

We thank the Koch Institute's Robert A. Swanson (1969) Biotechnology Center for their technical support, especially the Flow Cytometry Facility and MIT BioMicro Center. We thank S. Levine, N. Kamelamela, and G. Paradis for helpful discussions and suggestions. This work was supported in part by the Koch Institute Frontier Research Program through the Michael (1957) and Inara Erdei Fund and the Casey and Family Foundation Research Fund, the Packard Foundation, NIH Director's New Innovator Award (DP2-AI158126), U.S. Army Medical Research (W81XWH2210300), and Pfizer Inc. to M.E.B.; Hartford Foundation, Vitiligo Research Fund, NIH AATG T32 (AI132152), and NIH P50 (AR080593-01) to J.E.H.; a Canadian Institutes for Health Research Doctoral Foreign Study award to S.A.G.; a Medical Scientist Training Program grant (T32 GM007753) from the National Institute of General Medical Sciences to B.E.S.; a National Science Foundation Graduate Research Fellowship and fellowship from Ludwig Center at MIT's Koch Institute to C.R.P; and a graduate research fellowship from the Ludwig Center at MIT's Koch Institute to E.J.K.X. This work was delivered as part of the MATCHMAKERS team, of which M.E.B. is a member, supported by the Cancer Grand Challenges partnership financed by CRUK (CGCATF-2023/100001), the National Cancer Institute (OT2CA297463), and The Mark Foundation for Cancer Research. S.K.D. and H.S. are supported by the Hale Center for Pancreatic Cancer Research at Dana-Farber Cancer Institute (DFCI). S.K.D. is a member of the Parker Institute for Cancer Immunotherapy at DFCI. M.E.B. and S.K.D. are supported by Break Through Cancer. M.E.B. and M.D. are supported by the Bridge Project, a partnership between the Koch Institute for Integrative Cancer Research at MIT and the Dana-Farber/Harvard Cancer Center. This work was additionally supported in part by the Koch Institute Support (core) grant P30-CA14051 from the National Cancer Institute. Vitiligo samples were obtained from subjects who provided written consent to be included in Protocol H-14848. We would like to thank all our subjects who agreed to participate in this study. This content is solely the responsibility of the authors and does not necessarily represent the official views of the National Institutes of Health or the National Cancer Institute.

AUTHOR CONTRIBUTIONS

Conceptualization, S.A.G., R.S.M., and M.E.B.; methodology, all authors; data analysis, S.A.G., R.S.M., C.K., M.H.W., S.A.J., L.R.A., J.S., and P.V.H.; sample acquisition, E.L.K., K.J.G., L.R.A., J.S., H.S., M.G., M.D., S.K.D., and J.E.H.; writing, S.A.G., C.K., and M.E.B.; review and editing, all authors.

DECLARATION OF INTERESTS

M.E.B. is a founder, consultant, and equity holder of Kelonia Therapeutics and Abata Therapeutics and received research funding from Pfizer Inc. that partially funds this work. S.K.D. received research funding unrelated to this project from Novartis, Bristol-Myers Squibb, and Takeda and is a founder, science advisory board member, and equity holder in Kojin and has equity in Axxis Bio. M.D. has research funding from Eli Lilly; he has received consulting fees from Genentech, ORIC Pharmaceuticals, Partner Therapeutics, SQZ Biotech, AzurRx, Eli Lilly, Mallinckrodt Pharmaceuticals, Aditum, Foghorn Therapeutics, Palleon, and Moderna; and he is a member of the Scientific Advisory Board for Neoleukin Therapeutics, Veravas, and Cerberus Therapeutics and has equity in Axxis Bio. J.E.H. is a consultant (fees) for Alys Pharmaceuticals, Incyte, Avoro, Matchpoint Therapeutics, Vividion, AbbVie, Aclaris, Almirall, and Bain Capital; is an investigator (grants/research funding) for Incyte, Barinthus Bio NA, NexImmune, and Cour Pharma; is a founder (stock) of Villaris Therapeutics (acquired by Incyte) and Alys Pharmaceuticals; and serves as Chief Innovation Officer for Alys Pharmaceuticals. H.S. receives research funding from AstraZeneca, travel and boarding fees from Dava

Oncology, fees from UpToDate, and consulting fees from Dewpoint Therapeutics, Zola Therapeutics, and Merck, Sharpe, & Dohme. C.K., M.H.W., S.A.J., K.M.K., J.A.G., and A.W. are employed by Pfizer Inc. C.S.D. is an equity holder of Kelonia Therapeutics and is currently employed by Johnson & Johnson. P.V.H. is a founder, equity holder, and current employee of Fletcher Biosciences. C.R.P. is currently employed by TwoStep Therapeutics. C.S.D. and M.E.B. are co-inventors on patents related to this work filed by MIT: US Patents 12,061,187 (filed 23 March 2020, published 26 November 2020), 12,061,188 (filed 30 August 2023, published 8 February 2024), and 12,222,347 (filed 30 August 2023, published 11 July 2024).

STAR★METHODS

Detailed methods are provided in the online version of this paper and include the following:

- KEY RESOURCES TABLE
- EXPERIMENTAL MODEL AND SUBJECT DETAILS
  - Cell lines
  - Biological Samples
- METHOD DETAILS
  - Plasmid cloning and construction
  - Selection of TCRAFT Golden Gate overhang sets
  - Generation of TCRAFT CDR3 oligo pools
  - Validation of Golden Gate overhang sets
  - Synthesis and cloning of TCR libraries
  - TCR library and oligo pool sequencing
  - Single-cell RNA and TCR sequencing
  - Expression of TCRs in reporter Jurkat J76 cells
  - Library-versus-library RAPTR lentiviral screening assay
  - Peptide-APC and J76 library co-culture screen
  - Bulk sequencing of TCRs enriched by antigen screens
  - Individual functional TCR validation
- QUANTIFICATION AND STATISTICAL ANALYSES
  - Software

SUPPLEMENTAL INFORMATION

Supplemental information can be found online at https://doi.org/10.1016/j.immuni.2026.01.001.

Received: April 24, 2025
Revised: September 29, 2025
Accepted: December 31, 2025

REFERENCES

1. Joglekar, A.V., and Li, G. (2020). T cell antigen discovery. Nat. Methods *18*, 873–880. https://doi.org/10.1038/s41592-020-0867-z.
2. Hudson, D., Fernandes, R.A., Basham, M., Ogg, G., and Koohy, H. (2023). Can we predict T cell specificity with digital biology and machine learning? Nat. Rev. Immunol. *23*, 511–521. https://doi.org/10.1038/s41577-023-00835-3.
3. Robins, H.S., Srivastava, S.K., Campregher, P.V., Turtle, C.J., Andriesen, J., Riddell, S.R., Carlson, C.S., and Warren, E.H. (2010). Overlap and effective size of the human CD8+ T cell receptor repertoire. Sci. Transl. Med. *2*, 47ra64. https://doi.org/10.1126/scitranslmed.3001442.
4. Arstila, T.P., Casrouge, A., Baron, V., Even, J., Kanellopoulos, J., and Kourilsky, P. (1999). A direct estimate of the human alphabeta T cell receptor diversity. Science *286*, 958–961. https://doi.org/10.1126/science.286.5441.958.
5. Rosenberg, S.A., and Dudley, M.E. (2009). Adoptive cell therapy for the treatment of patients with metastatic melanoma. Curr. Opin. Immunol. *21*, 233–240. https://doi.org/10.1016/j.coi.2009.03.002.
6. Frick, R., Høydahl, L.S., Petersen, J., du Pré, M.F., Kumari, S., Berntsen, G., Dewan, A.E., Jeliazkov, J.R., Gunnarsen, K.S., Frigstad, T., et al. (2021). A high-affinity human TCR-like antibody detects celiac disease gluten peptide-MHC complexes and inhibits T cell activation. Sci. Immunol. *6*, eabg4925. https://doi.org/10.1126/sciimmunol.abg4925.
7. Oliveira, G., Stromhaug, K., Klaeger, S., Kula, T., Frederick, D.T., Le, P.M., Forman, J., Huang, T., Li, S., Zhang, W., et al. (2021). Phenotype, specificity and avidity of antitumour CD8+ T cells in melanoma. Nature *596*, 119–125. https://doi.org/10.1038/s41586-021-03704-y.
8. Ahmadzadeh, M., Johnson, L.A., Heemskerk, B., Wunderlich, J.R., Dudley, M.E., White, D.E., and Rosenberg, S.A. (2009). Tumor antigen-specific CD8 T cells infiltrating the tumor express high levels of PD-1 and are functionally impaired. Blood *114*, 1537–1544. https://doi.org/10.1182/blood-2008-12-195792.
9. Schumacher, T.N., and Schreiber, R.D. (2015). Neoantigens in cancer immunotherapy. Science *348*, 69–74. https://doi.org/10.1126/science.aaa4971.
10. Rosenberg, S.A., and Restifo, N.P. (2015). Adoptive cell transfer as personalized immunotherapy for human cancer. Science *348*, 62–68. https://doi.org/10.1126/science.aaa4967.
11. Dezfulian, M.H., Kula, T., Pranzatelli, T., Kamitaki, N., Meng, Q., Khatri, B., Perez, P., Xu, Q., Chang, A., Kohlgruber, A.C., et al. (2023). TScan-II: A genome-scale platform for the de novo identification of CD4+ T cell epitopes. Cell *186*, 5569–5586.e21. https://doi.org/10.1016/j.cell.2023.10.024.
12. Trouw, L.A., Rispens, T., and Toes, R.E.M. (2017). Beyond citrullination: other post-translational protein modifications in rheumatoid arthritis. Nat. Rev. Rheumatol. *13*, 331–339. https://doi.org/10.1038/nrrheum.2017.15.
13. Wang, J., Jelcic, I., Mühlenbruch, L., Haunerdinger, V., Toussaint, N.C., Zhao, Y., Cruciani, C., Faigle, W., Naghavian, R., Foege, M., et al. (2020). HLA-DR15 molecules jointly shape an autoreactive T cell repertoire in multiple sclerosis. Cell *183*, 1264–1281.e20. https://doi.org/10.1016/j.cell.2020.09.054.
14. Yee, C., Thompson, J.A., Roche, P., Byrd, D.R., Lee, P.P., Piepkorn, M., Kenyon, K., Davis, M.M., Riddell, S.R., and Greenberg, P.D. (2000). Melanocyte destruction after antigen-specific immunotherapy of melanoma: direct evidence of t cell-mediated vitiligo. J. Exp. Med. *192*, 1637–1644. https://doi.org/10.1084/jem.192.11.1637.
15. Mandelcorn-Monson, R.L., Shear, N.H., Yau, E., Sambhara, S., Barber, B.H., Spaner, D., and DeBenedette, M.A. (2003). Cytotoxic T lymphocyte reactivity to gp100, MelanA/MART-1, and tyrosinase, in HLA-A2-positive vitiligo patients. J. Investig. Dermatol. *121*, 550–556. https://doi.org/10.1046/j.1523-1747.2003.12413.x.
16. Le Gal, F.A., Avril, M.F., Bosq, J., Lefebvre, P., Deschemin, J.C., Andrieu, M., Dore, M.X., and Guillet, J.G. (2001). Direct evidence to support the role of antigen-specific CD8(+) T cells in melanoma-associated vitiligo. J. Investig. Dermatol. *117*, 1464–1470. https://doi.org/10.1046/j.0022-202x.2001.01605.x.
17. Cole, D.J., Weil, D.P., Shilyansky, J., Custer, M.C., Kawakami, Y., Rosenberg, S.A., and Nishimura, M.I. (1995). Characterization of the functional specificity of a cloned T-cell receptor heterodimer recognizing the MART 1 melanoma antigen. Cancer Res. *55*, 748–752.
18. Pai, J.A., and Satpathy, A.T. (2021). High throughput and single-cell T cell receptor sequencing technologies. Nat. Methods *18*, 881–892. https://doi.org/10.1038/s41592-021-01201-8.
19. Pogorelyy, M.V., Kirk, A.M., Adhikari, S., Minervina, A.A., Sundararaman, B., Vegesana, K., Brice, D.C., Scott, Z.B.; SJTRC Study Team, and Thomas, P.G. (2024). TIRTL-seq: Deep, quantitative, and affordable paired TCR repertoire sequencing. Preprint at bioRxiv. https://doi.org/10.1101/2024.09.16.613345.
20. Guo, X.-Z.J., Dash, P., Calverley, M., Tomchuck, S., Dallas, M.H., and Thomas, P.G. (2016). Rapid cloning, expression, and functional characterization of paired αβ and γδ T-cell receptor chains from single-cell analysis. Mol. Ther. Methods Clin. Dev. *3*, 15054. https://doi.org/10.1038/mtm.2015.54.

21. Zong, S., Mi, T., Flores, L.G., 2nd, Alpert, A., Olivares, S., Patel, K., Maiti, S., Mcnamara, G., Cooper, L.J.N., and Torikai, H. (2020). Very rapid cloning, expression and identifying specificity of T-cell receptors for T-cell engineering. PLoS One *15*, e0228112. https://doi.org/10.1371/journal.pone.0228112.

22. Hu, Z., Anandappa, A.J., Sun, J., Kim, J., Leet, D.E., Bozym, D.J., Chen, C., Williams, L., Shukla, S.A., Zhang, W., et al. (2018). A cloning and expression system to probe T-cell receptor specificity and assess functional avidity to neoantigens. Blood *132*, 1911–1921. https://doi.org/10.1182/blood-2018-04-843763.

23. Xia, Q., Huang, H., and Davis, M.M. (2022). A high-throughput strategy for T-cell receptor cloning and expression. Methods Mol. Biol. *2574*, 251–264. https://doi.org/10.1007/978-1-0716-2712-9_12.

24. Afeyan, A.B., Wu, C.J., and Oliveira, G. (2025). Rapid parallel reconstruction and specificity screening of hundreds of T cell receptors. Nat. Protoc. *20*, 539–586. https://doi.org/10.1038/s41596-024-01061-4.

25. Messemaker, M., Kwee, B.P.Y., Moravec, Ž., Álvarez-Salmoral, D., Urbanus, J., de Paauw, S., Geerligs, J., Voogd, R., Morris, B., Guislain, A., et al. (2025). A functionally validated TCR-pMHC database for TCR specificity model development. Preprint at bioRxiv. https://doi.org/10.1101/2025.04.28.651095.

26. Hamberger, M., Neuhoff, M.-T., Pietrantonio, S.V., Boschert, T., Torres, C. M., Errerd, A., Tan, C.L., Lindner, J.M., Platten, M., and Green, E.W. (2025). MakeTCR: A modular platform for rapid, flexible, scalable, single-step T cell receptor synthesis. Preprint at bioRxiv. https://doi.org/10.1101/2025.04.27.647198.

27. Genolet, R., Bobisse, S., Chiffelle, J., Arnaud, M., Petremand, R., Queiroz, L., Michel, A., Reichenbach, P., Cesbron, J., Auger, A., et al. (2023). TCR sequencing and cloning methods for repertoire analysis and isolation of tumor-reactive TCRs. Cell Rep. Methods *3*, 100459. https://doi.org/10.1016/j.crmeth.2023.100459.

28. Fahad, A.S., Chung, C.-Y., Lopez Acevedo, S.N., Boyle, N., Madan, B., Gutiérrez-González, M.F., Matus-Nicodemos, R., Laflin, A.D., Ladi, R.R., Zhou, J., et al. (2022). Immortalization and functional screening of natively paired human T cell receptor repertoires. Protein Eng. Des. Sel. *35*, gzab034. https://doi.org/10.1093/protein/gzab034.

29. Spindler, M.J., Nelson, A.L., Wagner, E.K., Oppermans, N., Bridgeman, J. S., Heather, J.M., Adler, A.S., Asensio, M.A., Edgar, R.C., Lim, Y.W., et al. (2020). Massively parallel interrogation and mining of natively paired human TCRαβ repertoires. Nat. Biotechnol. *38*, 609–619. https://doi.org/10.1038/s41587-020-0438-y.

30. Kuilman, T., Schrikkema, D.S., Gadiot, J., Gomez-Eerland, R., Bies, L., Walker, J., Spaapen, R.M., Kok, H., Houg, D., Viyacheva, M., et al. (2025). Enabling next-generation engineered TCR-T therapies based on high-throughput TCR discovery from diagnostic tumor biopsies. Nat. Commun. *16*, 649. https://doi.org/10.1038/s41467-024-55420-6.

31. Moravec, Z., Zhao, Y., Voogd, R., Cook, D.R., Kinrot, S., Capra, B., Yang, H., Raud, B., Ou, J., Xuan, J., et al. (2024). Discovery of tumor-reactive T cell receptors by massively parallel library synthesis and screening. Nat. Biotechnol. *43*, 214–222. https://doi.org/10.1038/s41587-024-02210-6.

32. Dobson, C.S., Reich, A.N., Gaglione, S., Smith, B.E., Kim, E.J., Dong, J., Ronsard, L., Okonkwo, V., Lingwood, D., Dougan, M., et al. (2022). Antigen identification and high-throughput interaction mapping by reprogramming viral entry. Nat. Methods *19*, 449–460. https://doi.org/10.1038/s41592-022-01436-z.

33. Pryor, J.M., Potapov, V., Kucera, R.B., Bilotti, K., Cantor, E.J., and Lohman, G.J.S. (2020). Enabling one-pot Golden Gate assemblies of unprecedented complexity using data-optimized assembly design. PLoS One *15*, e0238592. https://doi.org/10.1371/journal.pone.0238592.

34. Ogg, G.S., Rod Dunbar, P., Romero, P., Chen, J.L., and Cerundolo, V. (1998). High frequency of skin-homing melanocyte-specific cytotoxic T lymphocytes in autoimmune vitiligo. J. Exp. Med. *188*, 1203–1208. https://doi.org/10.1084/jem.188.6.1203.

35. Strassner, J.P., Rashighi, M., Ahmed Refat, M., Richmond, J.M., and Harris, J.E. (2017). Suction blistering the lesional skin of vitiligo patients reveals useful biomarkers of disease activity. J. Am. Acad. Dermatol. *76*, 847–855.e5. https://doi.org/10.1016/j.jaad.2016.12.021.

36. van den Boorn, J.G., Konijnenberg, D., Dellemijn, T.A.M., van der Veen, J. P.W., Bos, J.D., Melief, C.J.M., Vyth-Dreese, F.A., and Luiten, R.M. (2009). Autoimmune destruction of skin melanocytes by perilesional T cells from vitiligo patients. J. Investig. Dermatol. *129*, 2220–2232. https://doi.org/10.1038/jid.2009.32.

37. Lang, K.S., Caroli, C.C., Muhm, A., Wernet, D., Moris, A., Schittek, B., Knauss-Scherwitz, E., Stevanovic, S., Rammensee, H.G., and Garbe, C. (2001). HLA-A2 restricted, melanocyte-specific CD8(+) T lymphocytes detected in vitiligo patients are related to disease activity and are predominantly directed against MelanA/MART1. J. Investig. Dermatol. *116*, 891–897. https://doi.org/10.1046/j.1523-1747.2001.01363.x.

38. Li, Z., Ren, J., Niu, X., Xu, Q., Wang, X., Liu, Y., and Xiao, S. (2016). Meta-analysis of the association between vitiligo and human leukocyte antigen-A. BioMed Res. Int. *2016*, 5412806. https://doi.org/10.1155/2016/5412806.

39. Rosskopf, S., Leitner, J., Paster, W., Morton, L.T., Hagedoorn, R.S., Steinberger, P., and Heemskerk, M.H.M. (2018). A Jurkat 76 based triple parameter reporter system to evaluate TCR functions and adoptive T cell strategies. Oncotarget *9*, 17608–17619. https://doi.org/10.18632/oncotarget.24807.

40. Bentzen, A.K., Marquard, A.M., Lyngaa, R., Saini, S.K., Ramskov, S., Donia, M., Such, L., Furness, A.J.S., McGranahan, N., Rosenthal, R., et al. (2016). Large-scale detection of antigen-specific T cells using peptide-MHC-I multimers labeled with DNA barcodes. Nat. Biotechnol. *34*, 1037–1045. https://doi.org/10.1038/nbt.3662.

41. Ma, K.-Y., Schonnesen, A.A., He, C., Xia, A.Y., Sun, E., Chen, E., Sebastian, K.R., Guo, Y.-W., Balderas, R., Kulkarni-Date, M., et al. (2021). High throughput and high-dimensional single-cell analysis of antigen-specific CD8+ T cells. Nat. Immunol. *22*, 1590–1598. https://doi.org/10.1038/s41590-021-01073-2.

42. Yu, B., Shi, Q., Belk, J.A., Yost, K.E., Parker, K.R., Li, R., Liu, B.B., Huang, H., Lingwood, D., Greenleaf, W.J., et al. (2022). Engineered cell entry links receptor biology with single-cell genomics. Cell *185*, 4904–4920.e22. https://doi.org/10.1016/j.cell.2022.11.016.

43. Guo, X.J., and Elledge, S.J. (2022). V-CARMA: A tool for the detection and modification of antigen-specific T cells. Proc. Natl. Acad. Sci. USA *119*, e2116277119. https://doi.org/10.1073/pnas.2116277119.

44. Gangaev, A., Rozeman, E.A., Rohaan, M.W., Isaeva, O.I., Philips, D., Patiwael, S., van den Berg, J.H., Ribas, A., Schadendorf, D., Schilling, B., et al. (2021). Differential effects of PD-1 and CTLA-4 blockade on the melanoma-reactive CD8 T cell response. Proc. Natl. Acad. Sci. USA *118*, e2102849118. https://doi.org/10.1073/pnas.2102849118.

45. Vita, R., Blazeska, N., Marrama, D., IEDB Curation Team Members, Duesing, S., Bennett, J., Greenbaum, J., De Almeida Mendes, M., Mahita, J., Wheeler, D.K., et al. (2025). The Immune Epitope Database (IEDB): 2024 update. Nucleic Acids Res *53*, D436–D443.

46. Andersen, R.S., Thrue, C.A., Junker, N., Lyngaa, R., Donia, M., Ellebæk, E., Svane, I.M., Schumacher, T.N., Thor Straten, P., and Hadrup, S.R. (2012). Dissection of T-cell antigen specificity in human melanoma. Cancer Res. *72*, 1642–1650. https://doi.org/10.1158/0008-5472.CAN-11-2614.

47. Murata, K., Nakatsugawa, M., Rahman, M.A., Nguyen, L.T., Millar, D.G., Mulder, D.T., Sugata, K., Saijo, H., Matsunaga, Y., Kagoya, Y., et al. (2020). Landscape mapping of shared antigenic epitopes and their cognate TCRs of tumor-infiltrating T lymphocytes in melanoma. eLife *9*, e53244. https://doi.org/10.7554/eLife.53244.

48. Reynisson, B., Alvarez, B., Paul, S., Peters, B., and Nielsen, M. (2020). NetMHCpan-4.1 and NetMHCIIpan-4.0: improved predictions of MHC antigen presentation by concurrent motif deconvolution and integration of MS MHC eluted ligand data. Nucleic Acids Res. *48*, W449–W454. https://doi.org/10.1093/nar/gkaa379.

49. Frisoli, M.L., Essien, K., and Harris, J.E. (2020). Vitiligo: Mechanisms of pathogenesis and treatment. Annu. Rev. Immunol. *38*, 621–648. https://doi.org/10.1146/annurev-immunol-100919-023531.

50. Collier, J.L., Weiss, S.A., Pauken, K.E., Sen, D.R., and Sharpe, A.H. (2021). Not-so-opposite ends of the spectrum: CD8+ T cell dysfunction across chronic infection, cancer and autoimmunity. Nat. Immunol. *22*, 809–819. https://doi.org/10.1038/s41590-021-00949-7.

51. Krishna, C., DiNatale, R.G., Kuo, F., Srivastava, R.M., Vuong, L., Chowell, D., Gupta, S., Vanderbilt, C., Purohit, T.A., Liu, M., et al. (2021). Single-cell sequencing links multiregional immune landscapes and tissue-resident T cells in ccRCC to tumor topology and therapy efficacy. Cancer Cell *39*, 662–677.e6. https://doi.org/10.1016/j.ccell.2021.03.007.

52. Riding, R.L., and Harris, J.E. (2019). The role of memory CD8+ T cells in vitiligo. J. Immunol. *203*, 11–19. https://doi.org/10.4049/jimmunol.1900027.

53. Baptista, A.P., Gola, A., Huang, Y., Milanez-Almeida, P., Torabi-Parizi, P., Urban, J.F., Jr., Shapiro, V.S., Gerner, M.Y., and Germain, R.N. (2019). The chemoattractant receptor Ebi2 drives intranodal naive CD4+ T cell peripheralization to promote effective adaptive immunity. Immunity *50*, 1188–1201.e6. https://doi.org/10.1016/j.immuni.2019.04.001.

54. Lowery, F.J., Krishna, S., Yossef, R., Parikh, N.B., Chatani, P.D., Zacharakis, N., Parkhurst, M.R., Levin, N., Sindiri, S., Sachs, A., et al. (2022). Molecular signatures of antitumor neoantigen-reactive T cells from metastatic human cancers. Science *375*, 877–884. https://doi.org/10.1126/science.abl5447.

55. Jonsson, A.H., Zhang, F., Dunlap, G., Gomez-Rivas, E., Watts, G.F.M., Faust, H.J., Rupani, K.V., Mears, J.R., Meednu, N., Wang, R., et al. (2022). Granzyme K+ CD8 T cells form a core population in inflamed human tissue. Sci. Transl. Med. *14*, eabo0686. https://doi.org/10.1126/scitranslmed.abo0686.

56. Lan, F., Li, J., Miao, W., Sun, F., Duan, S., Song, Y., Yao, J., Wang, X., Wang, C., Liu, X., et al. (2025). GZMK-expressing CD8+ T cells promote recurrent airway inflammatory diseases. Nature *638*, 490–498. https://doi.org/10.1038/s41586-024-08395-9.

57. Wallimann, A., and Schenk, M. (2023). IL-32 as a potential biomarker and therapeutic target in skin inflammation. Front. Immunol. *14*, 1264236. https://doi.org/10.3389/fimmu.2023.1264236.

58. Gellatly, K.J., Strassner, J.P., Essien, K., Refat, M.A., Murphy, R.L., Coffin-Schmitt, A., Pandya, A.G., Tovar-Garza, A., Frisoli, M.L., Fan, X., et al. (2021). scRNA-seq of human vitiligo reveals complex networks of subclinical immune activation and a role for CCR5 in Treg function. Sci. Transl. Med. *13*, eabd8995. https://doi.org/10.1126/scitranslmed.abd8995.

59. Rashighi, M., Agarwal, P., Richmond, J.M., Harris, T.H., Dresser, K., Su, M.-W., Zhou, Y., Deng, A., Hunter, C.A., Luster, A.D., et al. (2014). CXCL10 is critical for the progression and maintenance of depigmentation in a mouse model of vitiligo. Sci. Transl. Med. *6*, 223ra23. https://doi.org/10.1126/scitranslmed.3007811.

60. Okła, K., Farber, D.L., and Zou, W. (2021). Tissue-resident memory T cells in tumor immunity and immunotherapy. J. Exp. Med. *218*, e20201605. https://doi.org/10.1084/jem.20201605.

61. Richmond, J.M., Strassner, J.P., Zapata, L., Jr., Garg, M., Riding, R.L., Refat, M.A., Fan, X., Azzolino, V., Tovar-Garza, A., Tsurushita, N., et al. (2018). Antibody blockade of IL-15 signaling has the potential to durably reverse vitiligo. Sci. Transl. Med. *10*, eaam7710. https://doi.org/10.1126/scitranslmed.aam7710.

62. Cheuk, S., Schlums, H., Gallais Sérézal, I., Martini, E., Chiang, S.C., Marquardt, N., Gibbs, A., Detlofsson, E., Introini, A., Forkel, M., et al. (2017). CD49a expression defines tissue-resident CD8+ T cells poised for cytotoxic function in human skin. Immunity *46*, 287–300. https://doi.org/10.1016/j.immuni.2017.01.009.

63. Borgers, J.S.W., Lenkala, D., Kohler, V., Jackson, E.K., Linssen, M.D., Hymson, S., McCarthy, B., O'Reilly Cosgrove, E., Balogh, K.N., Esaulova, E., et al. (2025). Personalized, autologous neoantigen-specific T cell therapy in metastatic melanoma: a phase 1 trial. Nat. Med. *31*, 881–893. https://doi.org/10.1038/s41591-024-03418-4.

64. Yang, X., Garner, L.I., Zvyagin, I.V., Paley, M.A., Komech, E.A., Jude, K.M., Zhao, X., Fernandes, R.A., Hassman, L.M., Paley, G.L., et al. (2022). Autoimmunity-associated T cell receptors recognize HLA-B*27-bound peptides. Nature *612*, 771–777. https://doi.org/10.1038/s41586-022-05501-7.

65. Dash, P., Fiore-Gartland, A.J., Hertz, T., Wang, G.C., Sharma, S., Souquette, A., Crawford, J.C., Clemens, E.B., Nguyen, T.H.O., Kedzierska, K., et al. (2017). Quantifiable predictive features define epitope-specific T cell receptor repertoires. Nature *547*, 89–93. https://doi.org/10.1038/nature22383.

66. Ali, L.R., Lenehan, P.J., Cardot-Ruffino, V., Dias Costa, A., Katz, M.H.G., Bauer, T.W., Nowak, J.A., Wolpin, B.M., Abrams, T.A., Patel, A., et al. (2024). PD-1 blockade induces reactivation of nonproductive T-cell responses characterized by NF-κB signaling in patients with pancreatic cancer. Clin. Cancer Res. *30*, 542–553. https://doi.org/10.1158/1078-0432.CCR-23-1444.

67. Katz, M.H.G., Petroni, G.R., Bauer, T., Reilley, M.J., Wolpin, B.M., Stucky, C.-C., Bekaii-Saab, T.S., Elias, R., Merchant, N., Dias Costa, A., et al. (2023). Multicenter randomized controlled trial of neoadjuvant chemoradiotherapy alone or in combination with pembrolizumab in patients with resectable or borderline resectable pancreatic adenocarcinoma. J. Immunother. Cancer *11*, e007586. https://doi.org/10.1136/jitc-2023-007586.

68. Goncharov, M., Bagaev, D., Shcherbinin, D., Zvyagin, I., Bolotin, D., Thomas, P.G., Minervina, A.A., Pogorelyy, M.V., Ladell, K., McLaren, J. E., et al. (2022). VDJdb in the pandemic era: a compendium of T cell receptors specific for SARS-CoV-2. Nat. Methods *19*, 1017–1019. https://doi.org/10.1038/s41592-022-01578-0.

69. Trautmann, L., Rimbert, M., Echasserieau, K., Saulquin, X., Neveu, B., Dechanet, J., Cerundolo, V., and Bonneville, M. (2005). Selection of T cell clones expressing high-affinity public TCRs within Human cytomegalovirus-specific CD8 T cell responses. J. Immunol. *175*, 6123–6132. https://doi.org/10.4049/jimmunol.175.9.6123.

70. Oliveira, G., Stromhaug, K., Cieri, N., Iorgulescu, J.B., Klaeger, S., Wolff, J. O., Rachimi, S., Chea, V., Krause, K., Freeman, S.S., et al. (2022). Landscape of helper and regulatory antitumour CD4+ T cells in melanoma. Nature *605*, 532–538. https://doi.org/10.1038/s41586-022-04682-5.

71. Mangani, D., Yang, D., and Anderson, A.C. (2023). Learning from the nexus of autoimmunity and cancer. Immunity *56*, 256–271. https://doi.org/10.1016/j.immuni.2023.01.022.

72. Saggau, C., Bacher, P., Esser, D., Rasa, M., Meise, S., Mohr, N., Kohlstedt, N., Hutloff, A., Schacht, S.-S., Dargvainiene, J., et al. (2024). Autoantigen-specific CD4+ T cells acquire an exhausted phenotype and persist in human antigen-specific autoimmune diseases. Immunity *57*, 2416–2432.e8. https://doi.org/10.1016/j.immuni.2024.08.005.

73. Ferguson, J., Eleftheriadou, V., and Nesnas, J. (2023). Risk of melanoma and nonmelanoma skin cancer in people with vitiligo: United Kingdom population-based cohort study. J. Investig. Dermatol. *143*, 2204–2210. https://doi.org/10.1016/j.jid.2023.04.013.

74. Li, G., Bethune, M.T., Wong, S., Joglekar, A.V., Leonard, M.T., Wang, J.K., Kim, J.T., Cheng, D., Peng, S., Zaretsky, J.M., et al. (2019). T cell antigen discovery via trogocytosis. Nat. Methods *16*, 183–190. https://doi.org/10.1038/s41592-018-0305-7.

75. Joglekar, A.V., Leonard, M.T., Jeppson, J.D., Swift, M., Li, G., Wong, S., Peng, S., Zaretsky, J.M., Heath, J.R., Ribas, A., et al. (2019). T cell antigen discovery via signaling and antigen-presenting bifunctional receptors. Nat. Methods *16*, 191–198. https://doi.org/10.1038/s41592-018-0304-8.

76. Quiñones-Parra, S.M., Gras, S., Nguyen, T.H.O., Farenc, C., Szeto, C., Rowntree, L.C., Chaurasia, P., Sant, S., Boon, A.C.M., Jayasinghe, D., et al. (2025). Molecular determinants of cross-strain influenza A virus recognition by αβ T cell receptors. Sci. Immunol. *10*, eadn3805. https://doi.org/10.1126/sciimmunol.adn3805.

77. Wang, Y., Wang, Z., Yang, J., Lei, X., Liu, Y., Frankiw, L., Wang, J., and Li, G. (2024). Deciphering membrane-protein interactions and high-throughput antigen identification with cell doublets. Adv. Sci. (Weinh) *11*, e2305750. https://doi.org/10.1002/advs.202305750.

78. Kohlgruber, A.C., Dezfulian, M.H., Sie, B.M., Wang, C.I., Kula, T., Laserson, U., Larman, H.B., and Elledge, S.J. (2024). High-throughput discovery of MHC class I- and II-restricted T cell epitopes using synthetic cellular circuits. Nat. Biotechnol. *43*, 623–634. https://doi.org/10.1038/s41587-024-02248-6.

79. Kula, T., Dezfulian, M.H., Wang, C.I., Abdelfattah, N.S., Hartman, Z.C., Wucherpfennig, K.W., Lyerly, H.K., and Elledge, S.J. (2019). T-Scan: A genome-wide method for the systematic discovery of T cell epitopes. Cell *178*, 1016–1028.e13. https://doi.org/10.1016/j.cell.2019.07.009.

80. Kisielow, J., Obermair, F.-J., and Kopf, M. (2019). Deciphering CD4+ T cell specificity using novel MHC-TCR chimeric receptors. Nat. Immunol. *20*, 652–662. https://doi.org/10.1038/s41590-019-0335-z.

81. Hondowicz, B.D., Schwedhelm, K.V., Kas, A., Tasch, M.A., Rawlings, C., Ramchurren, N., McIntosh, M., D'Amico, L.A., Sanda, S., Standifer, N.E., et al. (2012). Discovery of T cell antigens by high-throughput screening of synthetic minigene libraries. PLoS One *7*, e29949. https://doi.org/10.1371/journal.pone.0029949.

82. Lemieux, A., Sannier, G., Nicolas, A., Nayrac, M., Delgado, G.-G., Cloutier, R., Brassard, N., Laporte, M., Duchesne, M., Sreng Flores, A.M., et al. (2024). Enhanced detection of antigen-specific T cells by a multiplexed AIM assay. Cell Rep. Methods *4*, 100690. https://doi.org/10.1016/j.crmeth.2023.100690.

83. Dadonaite, B., Crawford, K.H.D., Radford, C.E., Farrell, A.G., Yu, T.C., Hannon, W.W., Zhou, P., Andrabi, R., Burton, D.R., Liu, L., et al. (2023). A pseudovirus system enables deep mutational scanning of the full SARS-CoV-2 spike. Cell *186*, 1263–1278.e20. https://doi.org/10.1016/j.cell.2023.02.001.

84. Raguram, A., An, M., Chen, P.Z., and Liu, D.R. (2024). Directed evolution of engineered virus-like particles with improved production and transduction efficiencies. Nat. Biotechnol. *43*, 1635–1647. https://doi.org/10.1038/s41587-024-02467-x.

85. Hao, Y., Hao, S., Andersen-Nissen, E., Mauck, W.M., 3rd, Zheng, S., Butler, A., Lee, M.J., Wilk, A.J., Darby, C., Zager, M., et al. (2021). Integrated analysis of multimodal single-cell data. Cell *184*, 3573–3587. e29. https://doi.org/10.1016/j.cell.2021.04.048.

86. MacDonald, E.A., Katz, E.L., Pearson, T.F., and Harris, J.E. (2024). Performing suction blister skin biopsies. Curr. Protoc. *4*, e1073. https://doi.org/10.1002/cpz1.1073.

87. Manso, T., Folch, G., Giudicelli, V., Jabado-Michaloud, J., Kushwaha, A., Nguefack Ngoune, V., Georga, M., Papadaki, A., Debbagh, C., Pégorier, P., et al. (2022). IMGT® databases, related tools and web resources through three main axes of research and development. Nucleic Acids Res. *50*, D1262–D1272. https://doi.org/10.1093/nar/gkab1136.

88. Finak, G., McDavid, A., Yajima, M., Deng, J., Gersuk, V., Shalek, A.K., Slichter, C.K., Miller, H.W., McElrath, M.J., Prlic, M., et al. (2015). MAST: a flexible statistical framework for assessing transcriptional changes and characterizing heterogeneity in single-cell RNA sequencing data. Genome Biol. *16*, 278. https://doi.org/10.1186/s13059-015-0844-5.

89. Korsunsky, I., Millard, N., Fan, J., Slowikowski, K., Zhang, F., Wei, K., Baglaenko, Y., Brenner, M., Loh, P.-R., and Raychaudhuri, S. (2019). Fast, sensitive and accurate integration of single-cell data with Harmony. Nat. Methods *16*, 1289–1296. https://doi.org/10.1038/s41592-019-0619-0.

90. Lizio, M., Harshbarger, J., Shimoji, H., Severin, J., Kasukawa, T., Sahin, S., Abugessaisa, I., Fukuda, S., Hori, F., Ishikawa-Kato, S., et al. (2015). Gateways to the FANTOM5 promoter level mammalian expression atlas. Genome Biol. *16*, 22. https://doi.org/10.1186/s13059-014-0560-6.

91. GTEx Consortium (2013). The Genotype-Tissue Expression (GTEx) project. Nat. Genet. *45*, 580–585. https://doi.org/10.1038/ng.2653.

92. Belote, R.L., Le, D., Maynard, A., Lang, U.E., Sinclair, A., Lohman, B.K., Planells-Palop, V., Baskin, L., Tward, A.D., Darmanis, S., et al. (2021). Human melanocyte development and melanoma dedifferentiation at single-cell resolution. Nat. Cell Biol. *23*, 1035–1047. https://doi.org/10.1038/s41556-021-00740-8.

Please cite this article in press as: Gaglione et al., Scalable TCR synthesis and screening enable antigen reactivity mapping in vitiligo, Immunity (2026), https://doi.org/10.1016/j.immuni.2026.01.001

STAR★METHODS

KEY RESOURCES TABLE

REAGENT or RESOURCE	SOURCE	IDENTIFIER
Antibodies		
APC anti-human CD69 (clone FN50)	Biolegend	Cat#310910; RRID: AB_314845
PE anti-human CD19 (clone HIB19)	Biolegend	Cat#302208; RRID: AB_314238
APC anti-human TCR α/β (clone IP26)	Biolegend	Cat#306718; RRID: AB_10612569
PE anti-human TCR α/β (clone IP26)	Biolegend	Cat#306708; RRID: AB_314646
Bacterial and virus strains		
Stbl3 chemical competent cells	ThermoFisher	Cat#C737303
ElectroMAX® DH10β electrocompetent E. coli	ThermoFisher	Cat#18290015
Biological samples		
Suction blister biopsies	Vitiligo Clinic and Research Center, University of Massachusetts Chan Medical School	N/A
Chemicals, peptides, and recombinant proteins		
Synthesized peptides	Genscript	Table S2
Phorbol 12-myristate 13-acetate (PMA)	ThermoFisher	Cat#J63916.MA
DEAE-dextran hydrochloride	Sigma	Cat#D9885-10G
Ionomycin, 96%	ThermoFisher	Cat#J62448.MCR
Critical commercial assays		
NEBNext Ultra II Q5 Master Mix	NEB	Cat#M0544L
KAPA HiFi HotStart Readymix	Roche	Cat# KK2601
NEBridge Ligase Master Mix	NEB	Cat#M1100
NEBridge Golden Gate Assembly Kit (BsmBI-v2)	NEB	Cat#E1602
NEBridge Golden Gate Assembly Kit (BsaI-HF-v2)	NEB	Cat#E1601
BsaI-HF-v2	NEB	Cat#R3733
BsmBI-v2	NEB	Cat#R0739
BbsI-HF	NEB	Cat#R3539
SapI	NEB	Cat#R0569
FastDigest XbaI	ThermoFisher	Cat#FD0685
FastDigest Buffer	ThermoFisher	Cat#B64
Nuclease-free water (not DEPC-treated)	ThermoFisher	Cat#AM9937
Shrimp alkaline phosphatase (rSAP)	NEB	Cat#M0371
ElectroMAX DH10B E. coli	ThermoFisher	Cat#18290015
MCE membrane filter, 0.025 μm pore size	Millipore Sigma	Cat#VSWP02500
Chloramphenicol	Millipore Sigma	Cat#C0378
Electroporation cuvette (1 mm gap)	VWR	Cat#89047-206
SPRIselect beads	Beckman Coulter	Cat#B23317
GeneJET Plasmid Miniprep Kit	ThermoFisher	Cat#K0502
GeneJET Gel Extraction Kit	ThermoFisher	Cat#K0692
TransIT®-Lenti Transfection Reagent	Millipore Sigma	Cat#MIR6603
Quikchange Lightning Site-Directed Mutagenesis Kit	Agilent	Cat#210518
Genscript Genbuilder Gibson Mix	Genscript	Cat#L00701-50
Ligation sequencing DNA V14	Oxford Nanopore Technologies	Cat#SQK-LSK114
Chromium GEM-X Single Cell 5′ Kit v3	10X Genomics	Cat#PN-1000695
Chromium Next GEM Single Cell 5′ Kit v2	10X Genomics	Cat#PN-1000263

(*Continued on next page*)

Please cite this article in press as: Gaglione et al., Scalable TCR synthesis and screening enable antigen reactivity mapping in vitiligo, Immunity (2026), https://doi.org/10.1016/j.immuni.2026.01.001

Continued

REAGENT or RESOURCE	SOURCE	IDENTIFIER
Chromium Next GEM Single Cell 5′ Kit v1.1	10X Genomics	Cat#PN-1000165
Library Construction Kit	10X Genomics	Cat#PN-1000190
Chromium Single Cell Human TCR Amplification Kit	10X Genomics	Cat# PN-1000252
PureLink™ Genomic DNA Mini Kit	ThermoFisher	Cat#K182001
Deposited data		
Raw TCRAFT library sequencing (Nanopore and Element)	This paper	SRA: PRJNA1247142
Raw bulk NGS data (RAPTR)	This paper	SRA: PRJNA1247142
Raw single cell sequencing data (RAPTR)	This paper	SRA: PRJNA1247142
Processed blister fluid scTCR-seq and scRNA-seq data	This paper	https://singlecell.broadinstitute.org/single_cell: accession SCP3412
30,810 TCR sequences (scTCR-seq data)	Ali et al.[76], Katz et al.[77]	N/A
Melanoma scRNA-seq data	Oliveira et al.[7]	dbGaP: study ID 26121, accession phs001451.v3.p1
Experimental models: Cell lines		
HEK-293T	ATCC	Cat#CRL-3216
Jurkat J76	Heemskerk lab	N/A
T2	ATCC	Cat#CRL-1992
NFAT-CFP CD8$^+$ Jurkat J76	This paper	N/A
J76_3808 TCR library	This paper	N/A
J76_30,810 TCR library	This paper	N/A
Clonal TCR J76	This paper	N/A
Oligonucleotides		
Oligos for TCRAFT	This paper	Table S4
Oligos for library preparation	This paper	Table S4
Recombinant DNA		
psPAX2	Addgene	Cat#12260
pMD2.G	Addgene	Cat#12261
pMD2.VSVG-mut	Addgene	Cat#182229
pGGAselect	Addgene	Cat#195714
pLeAPS-GFP	Addgene	Cat#182230
pHIV-peptide-b2M-HLA-A0201 (SCT pMHCs)	This paper	N/A
pHIV-TCR (clonal TCRs)	This paper	N/A
TCRAFT TRAV-TRBC and TRBC-TRAV vectors	This paper; Addgene	Cat# #1000000264 and Cat#1000000271
Software and algorithms		
Cellranger (vX3.1)	10X Genomics	https://www.10xgenomics.com/support/software/cell-ranger/latest
Prism (v10)	Graphpad	https://www.graphpad.com/features
Flowjo (v.10.10.0)	BD	https://www.flowjo.com/
Seurat (v.4.4.0)	Hao et al.[85]	https://doi.org/10.1016/j.cell.2021.04.048
TCRAFT package	This paper	https://github.com/birnbaumlab/TCRAFT
Other		
Code and analyses	This paper	https://github.com/birnbaumlab/TCRAFT https://github.com/birnbaumlab/Gaglione-et-al-2025

EXPERIMENTAL MODEL AND SUBJECT DETAILS

Cell lines

HEK293T cells (ATCC CRL-11268) were cultured in DMEM (ATCC) supplemented with 10% fetal bovine serum (FBS; Atlanta biologics) and penicillin-streptomycin (Gibco). Jurkat J76 T cells, a Jurkat E6.1 cell line devoid of TCR alpha and beta chains, were a

gift from Dr. M. Heemskerk.[39] J76 cells and T2 cells (ATCC CRL-1992) were cultured in RPMI-1640 (ATCC) supplemented with 10% FBS and penicillin-streptomycin.

Biological Samples

Suction blister biopsies

Individuals with rapidly progressing, active vitiligo were recruited under an Institutional Review Board-approved protocol (H-14848) at the University of Massachusetts Chan Medical School. Participants with a diagnosis of vitiligo by clinical exam performed by a dermatologist and treatment-naive for more than 6 months were included for sampling. Clinical blistering sites were examined through suction blister biopsies focused on specific areas showing disease symptoms. Blisters were purposefully formed over confetti or trichrome lesions, incorporating both affected and surrounding skin to capture immune cells. Active lesions not characterized as confetti or trichrome were sampled at the border zone between depigmented and pigmented skin. Ten suction blisters were obtained and pooled for each patient, as previously described.[86]

METHOD DETAILS

Plasmid cloning and construction

Oligonucleotides were ordered from IDT (listed in Table S2), gene fragments were synthesized by Twist Biosciences and IDT, oligonucleotide pools were synthesized by Twist Biosciences (250-300 nt) and IDT (300-350 nt), and TCRAFT vectors were constructed by Genscript and Twist Biosciences. psPAX2 and pMD2.G were gifts from D. Trono (Addgene #12260 and #12259). pMD2.G-VSV-G-mut is available on Addgene as plasmid #182229.[32] TRBV-TRAC and TRBC-TRAV TCRAFT vectors were designed using native human sequences for TRBV and TRAV alleles from IMGT.[87] Vectors were assembled by Twist Biosciences: TRBV-TRAC in a pGGA cloning vector with chloramphenicol resistance and TRAC-P2A-TRAV in the pTwist Kan HC v2 cloning vector with kanamycin resistance (Table S1). A lentiviral expression vector (pHIV backbone) was constructed by inserting a gene fragment (IDT) encoding LacZ flanked by SapI recognition sites (5'-GCA-SapI site-LacZ-SapI site-ATC-3') using Genscript Genbuilder Gibson Mix (Genscript #L00701-50) and removing an undesired backbone SapI site with the Quikchange Lightning Site-Directed Mutagenesis Kit (Agilent #210518).

To generate pMHC-displaying lentiviruses, 101 pMHCs were cloned into a pHIV backbone by Genscript as single-chain trimers (SCT)[32] (HGH signal peptide-peptide-G4S linker-β2 microglobulin-HLA-A*02:01) with two cysteine mutations to stabilize peptide-MHC binding (Y84C in HLA-A2 and G2C in the G4S linker). Our previously described pLeAPS-GFP plasmid[32] was modified to include a 10X bead-compatible tag sequence (TSO)[42] and an extended 18 bp barcode via randomized primers.

Individual TCRs for validation were ordered as TRBV-TRBC-P2A-TRAV gene fragments (IDT) and assembled via Golden Gate into the same pHIV backbone described above, modified to contain the TRAC flanked by BsmBI recognition sites.

Selection of TCRAFT Golden Gate overhang sets

Unique, highly orthogonal overhangs were designed for each TRBV-TRAC (n = 48) and TRBC-TRAV (n = 45) vector to ensure each CDR3α and CDR3β pairs with correct alleles in hierarchical Golden Gate assembly reactions. To ensure that TCRAFT assembly products formed functional protein coding sequences, the overhangs assigned to each TRBV-TRAC and/or TRBC-TRAV vector were encoded within the V/C region coding sequences. Because each vector was assigned a unique overhang pair, the same 93 overhang pairs were conserved across all TCRAFT assemblies regardless of the composition of the CDR3 oligo pool, enabling reproducible assemblies across TCR libraries of all sizes and compositions.

To begin the overhang design process, all possible valid 4-bp overhangs were first identified in the last 8 amino acids of each native TRBV and TRAV sequence and the first 10 amino acids of the TRAC and TRBC via combinatorial codon shuffling. An overhang set $\Omega = \left(O_1^L, O_1^R\right), \ldots, \left(O_n^L, O_n^R\right)$ was defined as a set of n overhang pairs $\left(O_i^L, O_i^R\right)$, where O_i^L and O_i^R correspond to the left and right 4-bp overhangs assigned to vector i, respectively. All 4-bp overhangs were defined to be in 5'-3' orientation by default.

A NEB dataset of overhang ligation fidelities for all 256 possible 4-bp overhangs was used to computationally model overhang ligation.[33] This dataset was generated by incubating an oligonucleotide pool spanning all 256 possible 4-bp overhangs with various Golden Gate Type IIS enzymes to measure the pairwise ligation fidelity between all possible 4-bp sequences. Because pairing fidelity was determined via sequencing of the ligated products, for all possible 4-bp overhang pairs O_i and O_j, the NEB dataset contains $r(O_i, O_j)$, the number of sequencing reads corresponding to O_i and O_j ligated together. By definition, r is symmetric: $r(O_i, O_j) = r(O_j, O_i)$.

The NEB ligation fidelity dataset was used to compute $p(O_i \mid \mathbb{S})$, the marginal probability that overhang O_i ligates with its Watson-Crick overhang pair $RC(O_i)$ (where $RC(O_i)$ denotes the reverse complement of O_i) given an arbitrary list $\mathbb{S}$ of total overhangs present in the reaction mixture as follows:

$$p(O_i \mid \mathbb{S}) = \frac{1}{2}\left[\frac{r(O_i, RC(O_i))}{\sum_{O_s \in \mathbb{S}} r(O_i, O_s)} + \frac{r(O_i, RC(O_i))}{\sum_{O_s \in \mathbb{S}} r(RC(O_i), O_s)}\right]$$

Please cite this article in press as: Gaglione et al., Scalable TCR synthesis and screening enable antigen reactivity mapping in vitiligo, Immunity (2026), https://doi.org/10.1016/j.immuni.2026.01.001

$p(O_i \mid \mathbb{S})$ was computed by dividing the number of reads corresponding to O_i ligated with $RC(O_i)$ by the sum of reads corresponding to O_i or $RC(O_i)$ ligating with all possible overhangs in the total background list $\mathbb{S}$. The average of two terms accounts for numerical differences between the sums $\sum_{O_s \in \mathbb{S}} r(O_i, O_s)$ and $\sum_{O_s \in \mathbb{S}} r(RC(O_i), O_s)$, which in practice are similar but not identical. For the purposes of TCRAFT overhang optimization, the following three background overhang lists were defined and used:

$\mathbb{L} := \left\{ O_i^L, RC\left(O_i^L\right) \;\middle|\; 1 \le i \le |\Omega| \right\}$ (the set of all left overhangs and their reverse complements), $\mathbb{R} := \left\{ O_i^R, RC\left(O_i^R\right) \;\middle|\; 1 \le i \le |\Omega| \right\}$ (the set of all right overhangs and their reverse complements), $\mathbb{T} := \mathbb{L} \cup \mathbb{R}$ (the total set of all possible overhangs present in the reaction mixture).

These components were used to construct a custom scoring function, $f(\Omega)$, which was designed to output higher scores for overhang sets that are predicted to be highly orthogonal and to yield accurate vector assemblies. $f(\Omega)$ was constructed as a weighted average of two sub-scores $f_1(\Omega)$ and $f_2(\Omega)$ as shown below:

$$f_1(\Omega) = \min_{1 \le i \le |\Omega|} \left[p\left(O_i^L \mid \mathbb{T}\right) \cdot p\left(O_i^R \mid \mathbb{T}\right) \right]$$

$$f_2(\Omega) = \prod_{1 \le i \le |\Omega|} p\left(O_i^L \mid \mathbb{L}\right) \cdot p\left(O_i^R \mid \mathbb{R}\right)$$

$$f(\Omega) = w \cdot f_1(\Omega) + (1 - w) \cdot f_2(\Omega)$$

$f_1(\Omega)$ was designed to optimize for maximal correct circular vector assembly and was computed by taking the minimum of the correct assembly probability product across all vectors. Aggregating scores across each vector using the minimum instead of calculating an average or sum ensures that correct circular assembly values across vectors all exceed a minimum threshold. $f_2(\Omega)$ was added as a regularization term to reward overhang sets that contain highly orthogonal overhangs and was computed by taking the total product of the left-ligation probabilities for all left overhangs and the right-ligation probability for all right overhangs. $f_1(\Omega)$ and $f_2(\Omega)$ were combined via a weighting coefficient which was empirically set to $w = 0.5$.

A Markov Chain Monte Carlo (MCMC) sampling approach inspired by the Metropolis algorithm and Simulated Annealing was used to stochastically identify overhang sets that achieve high scores on the scoring metric $f(\Omega)$. Each iteration, the algorithm generated a new candidate overhang set Ω' by randomly selecting one overhang $O_i \in \Omega$ and replacing it with a different valid overhang for that position. The new overhang set was scored to obtain $f(\Omega')$, and the update was either accepted or rejected according to the Metropolis acceptance distribution P_{accept}:

$$P_{accept} = min\left(1, exp\left(\frac{f(\Omega') - f(\Omega)}{T}\right)\right)$$

Optimization was carried out in two fixed-temperature stages (unlike classical simulated annealing, which uses a time-varying temperature schedule). In the first stage, eight random initializations of the overhang set were generated by sampling from the space of valid overhangs for each position, and these initial seeds were independently optimized for 10,000 iterations at a fixed temperature of $T = 10^{-4}$. All optimization trajectories were automatically terminated early if there was no score update for 1,000 consecutive iterations. Following the first round, the overhang set with the highest score out of the eight parallel runs was selected for a second, focused optimization round. In this second round, eight copies of the best-scoring set from round 1 were again optimized in parallel at a higher temperature of $T = 10^{-3}$ for 5,000 iterations. The highest-scoring set across all optimization runs was returned as the final overhang set.

The result was a pair of 4-bp overhangs for each TRBC-TRAV and TRBV-TRAC fragment that preserves coding sequences. A total of four overhang sets were generated: two overhang sets for TRBV-TRAC vectors, and another two sets for TRBC-TRAV vectors, termed A and B for both. TRAV pool A includes TRAV1-1 to TRAV16 (22 alleles) and pool B includes TRAV17 to TRAV41 (23 alleles). TRBV pool A includes TRBV2 to TRBV7-8 (24 alleles) and pool B includes TRBV7-9 to TRBV30 (24 alleles). TRAV and TRBV alleles were split into two pools each to maximize assembly efficiency. Code implementation of the workflow described above, which was used to generate all overhangs, is provided at https://github.com/birnbaumlab/Gaglione-et-al-2025.

Generation of TCRAFT CDR3 oligo pools

CDR3 oligos for TCRAFT assembly were generated using a software package available at https://github.com/birnbaumlab/TCRAFT. The script accepts a CSV file containing TRAV, TRBV, TRAJ, TRBJ, CDR3α, and CDR3β regions as an input, and outputs a list of oligos to order, pre-split into A and B pools. Output oligos are also separated by length ($\le$ 300 bp and >300 bp) to simplify ordering.

The CDR3 oligo generation code begins by randomly sampling codons according to a human codon usage distribution table to generate nucleotide sequences that translate to the input CDR3α/β amino acid sequences. Following random nucleotide sampling, the script removes all TCRAFT-relevant restriction sites and homopolymer sequences greater than 5 nucleotides in length via synonymous codon shuffling. The final CDR3 oligo is created by concatenating the appropriate primer sequences, restriction sites, and TRAV/TRBV/TRAC/TRBC junction sites with embedded overhangs to the cleaned CDR3α/β nucleotide sequences. Generated CDR3

Please cite this article in press as: Gaglione et al., Scalable TCR synthesis and screening enable antigen reactivity mapping in vitiligo, Immunity (2026), https://doi.org/10.1016/j.immuni.2026.01.001

oligos are validated by a second script, also accessible at the link above, which simulates end-to-end TCRAFT assembly for each CDR3 oligo and ensures that the simulated TCRAFT assembly matches the desired input TCR clonotype in amino acid space and does not contain any extraneous restriction sites.

Validation of Golden Gate overhang sets

Computationally generated overhang sets were experimentally validated. Four pools of backbone library vectors were generated by inserting pools of oligos containing the overhang sets, BsmBI recognition sites, and a defined barcode for each overhang to enable computation of assembly fidelity into pGGAselect (Addgene #195714). Oligo pools representing eventual CDR3α/β oligos were flanked with BsmBI recognition sites, prescribed overhangs, and a unique barcode. Oligo pools were amplified according to manufacturer instructions (15 cycles).

Vectors and oligos for each overhang set were pooled in Golden Gate assembly reactions at a 4:1 molar insert-to-vector ratio with 2 μL of BsmBI Golden Gate Enzyme Mix (NEB) and T4 Ligase Buffer (NEB). Golden Gate reactions were cycled (30 cycles of 42C for 5 min, 16C for 5 min; 60C for 5 min, 80C for 20 min). 2 μL of the product was heat-shock transformed into competent Stbl3 *E. coli*, cultured under chloramphenicol (Sigma Aldrich) selection, and midiprepped. Amplicons of ligated insert and flanks were PCR-amplified (30 cycles) and submitted to Genewiz (Amplicon-EZ NGS). Comparison of barcodes adjacent to insert overhangs allowed for quantification of on-target versus off-target vector-insert pairing within each overhang set.

Synthesis and cloning of TCR libraries

TCR libraries were generated in hierarchical Golden Gate assembly reactions as follows. Oligo pools A and B (Twist for 250-300 nt, 97% of TCRs; IDT for oligos > 300 nt, 3% of TCRs) were generated by the oligo generation script. Oligo pools were re-suspended as directed by the manufacturer. If ordered with separate manufacturers (Twist for ≤ 300 bp and IDT for >300 bp), oligos pools were mixed proportionally prior to amplifying. 20 ng of each oligo pool was PCR-amplified using NEBNext Ultra II Q5 Master Mix (NEB Cat #M0544L) (98C for 30s; 12 cycles of 98C for 30s, 68C for 30s, 72C for 30s; 72C for 5 min) using Oligo_f and Oligo_r primers followed by a 1.8× SPRIselect bead (Beckman Coulter) cleanup and elution in elution buffer (Thermo Fisher).

In step 1, CDR3α/β oligo pools A and B were inserted into the TRBV-TRAC-containing vectors (A and B). In parallel, TRBV-TRAC vector pool A was reacted with CDR3α/β oligo pool A, and TRBV-TRAC vector pool B was reacted with CDR3α/β oligo pool B. The following were combined to generate two 15 μL reactions (A and B): 0.1 pmol of vector mix, 0.4 pmol CDR3α/β oligo pool, 5 μL NEBridge Ligase Master Mix (NEB), 1 μL BbsI-HF enzyme (NEB), and nuclease-free water (Thermo Fisher). Both Golden Gate reactions were completed: 60 cycles of 37C for 5 min, 16C for 5 min; 65C for 20 min; hold at 4C. Post-reaction, a clean-up cut was performed to ensure complete elimination of unreacted vector by adding 1 μL of BbsI-HF enzyme (NEB) and 1 μL of shrimp alkaline phosphatase (rSAP) (NEB) to the reaction mix and incubating at 37C for 1 hour followed by 65C for 20 minutes for heat inactivation.

The step 1 products were drop dialyzed for 3 hours on an MCE membrane filter (0.025 pore size) (Millipore Sigma). Dialyzed products were electroporated into ElectroMAX® DH10β electrocompetent *E. coli* (Thermo Fisher, cat No. 18290015) according to manufacturer instructions. Following overnight culture under chloramphenicol (Sigma Aldrich) selection, electroporation efficiency was evaluated, and products 1A and 1B were midiprepped using a NucleoBond Xtra Midi EF kit (Macherey-Nagel). A minimum of 1000× library coverage was achieved at each electroporation step. Step 1A and 1B products were mixed proportionally according to the number of oligos in each oligo pool, henceforth referred to as step 1 product (minimum 300 ng required).

In step 2, step 1 product was reacted with the TRBC-TRAV-containing vectors (A and B) to insert TRBC-P2A-TRAV fragments between CDR3β and CDR3α. For step 2A, the following were combined to generate a 20 μL reaction: 150 ng of step 1 product and TRBC-TRAV pool A at a 1:2 molar ratio (313 ng), 2 μL of T4 ligase buffer (NEB), 1 μL NEBridge BsmBI-HF-v2 Master Mix (NEB), and nuclease-free water (Thermo Fisher). For step 2B, the following were combined to generate a 20 μL reaction: 150 ng of step 1 product and TRBC-TRAV pool B at a 1:2 molar ratio (313 ng), 2 μL of T4 ligase buffer (NEB), 1 μL NEBridge BsaI-v2 Master Mix (NEB), and nuclease-free water (Thermo Fisher). Step 2A and 2B were completed separately with the following cycling conditions: 60 cycles of 42C (BsmBI, step 2A) or 37C (BsaI, step 2B) for 5 min, 60C for 5 min; 80C for 20 min; hold at 4C. Post-reaction, 1 μL of BsmBI-v2 enzyme (NEB) or 1 μL of BsaI-HF-v2 enzyme (NEB) were added to steps 2A and 2B, respectively, in addition to 1 μL of rSAP (NEB). Both were incubated at 55C (step 2A, BsmBI) or 37C (step 2B, BsaI) for 1 hour followed by 80C for 20 minutes. Step 2 products were dialyzed and electroporated identically as in step 1, described above, followed by culture under chloramphenicol (Sigma Aldrich) selection. Midiprepped step 2 products were mixed proportionally to form the complete TCR library (minimum 244 ng required).

In step 3, the complete synthetic TCR library was transferred to a destination lentiviral expression vector, described above, to enable TCR expression in cells. The following were combined to generate a 15 μL reaction: 0.05 pmol destination vector, 0.1 pmol of mixed step 2 product, 5 μL of NEBridge Ligase Master Mix (NEB), 1 μL of SapI enzyme (NEB), and nuclease-free water (Thermo Fisher). The following cycling conditions were used: 60 cycles of 37C for 5 min, 16C for 5 min; 60C for 5 min; hold at 4C. Immediately before dialyzing, the reaction was incubated at 60C for 5 min and 65C for 20 min to enable heat inactivation. The step 3 products were dialyzed and electroporated identically to steps 1 and 2, described above, followed by culture under carbenicillin (Sigma Aldrich) selection. The final product is a complete, pooled TCR library in a lentiviral expression vector.

TCR library and oligo pool sequencing

To examine and quantify assembled TCR sequences, TCR plasmid libraries and oligo pools were sequenced. Products of reactions 1, 2, and 3 contain several unique cut sites including XbaI. Products were digested with FastDigest XbaI (Thermo Fisher) in FastDigest

Buffer (Thermo Fisher) for one hour at 37C. The digested products were purified via columns by mixing products 1:1 with binding buffer from GeneJET Gel Extraction Kit and following kit instructions. Oxford Nanopore-compatible libraries were generated via ligation with kit SQK-LSK114 (ONT) and sequenced on a PromethION R10 flowcell (ONT). For the 3,808 TCR library, the intermediate products (reactions 1 and 2) and final product (reaction 3) were sequenced. For the 30,810 TCR library, only the final product (reaction 3) was sequenced. Long-read sequencing enables minimally biased evaluation of correct pairing, as it avoids PCR steps that depend on specific primer binding sites.

For greater read depth, short-read sequencing was used to sequence TRAV-CDR3α regions (primers: TRAV_CDR3A_f, TRAV_CDR3A_r), TRBV-CDR3β regions (primers: TRBV_CDR3B_f, TRBV_CDR3B_r), and CDR3α-CDR3β oligos (primers: Oligo_Illumina_f and Oligo_Illumina_r). All primers were used at 1 μM. PCRs were completed with NEBNext Ultra II Q5 Master Mix (NEB #M0544). CDR3α-CDR3β oligo pools were PCR-amplified to add partial Illumina adapters with the above primers (50 ng template; 98C for 30 sec; 13 cycles of 98C for 30 sec, 70C for 30 sec, 72C for 30 sec; 72C for 1 min). TRAV-CDR3α and TRBV-CDR3β regions were PCR-amplified with above primers binding conserved regions to add partial Illumina adapters. Template for this reaction consisted of plasmid library (50 ng); reaction conditions: 98C for 30 sec; 15 cycles of 98C for 30 sec, 70C for 30 sec, 72C for 45 sec; 72C for 1 min. A second PCR added indices and complete Illumina adapters to all amplicons (primers: Illumina_Truseq_f and Illumina_Truseq_r; 20–100 pg template; 98C for 30 sec; 15 cycles of 98C for 30 sec, 70C for 30 sec, 72C for 30 sec; 72C for 1 min). Amplicons were pooled in an equimolar manner and sequenced with an Element AVITI, generating paired end 300 bp reads.

Long-read sequence processing

Long-read sequencing analysis was completed in Python. Reads were filtered with a size cutoff 8500 bp for the final TCR library (step 3, size ~8800 bp), 2800 bp for step 1 product, and 3500 bp for step 2 product. To filter out non-TCR sequences, reads were filtered for the presence of a TRAC and TRBC. Next, each read was mapped to a TRAV and TRBV and sequences in the adjacent CDR3 regions were extracted. Each CDR3 region was independently searched for the designed CDR3α and CDR3β sequences; in addition to mapping CDR3α and CDR3β regions to the designed list, new CDR3α and CDR3β sequences were also annotated. Correctly paired, incorrectly paired, and new complete TCR sequences were recorded and counted. Downstream analysis and plots were generated with Matplotlib and Seaborn in Python.

Short-read sequence processing

Short read sequencing analysis was completed in Python. For CDR3 oligo pool sequencing data, forward and reverse reads were merged into a single contiguous read using the PEAR software package (v0.9.10). Following read merging, reads were annotated by performing an exact match dictionary search against oligo sequences ordered. For TRAV-CDR3α and TRBV-CDR3β amplicons, forward and reverse reads were processed independently. The reverse reads, which captured most of the CDR3, were used to extract and annotate the CDR3 coding sequence via exact match lookup.

Single-cell RNA and TCR sequencing

3,808 TCR library

scRNA-seq library generation. Blister fluid was centrifuged at 350g for 10 minutes at 4C. For single-cell sequencing, whole cell pellet from blisters was used for 10X input due to cell counts being significantly lower than maximum cell input recommendation. Once the single cell suspension was obtained, samples were processed using the standard chromium 5′ V1 (VB203 donor) or V2 (others) + TCR library generation workflow (10x Genomics) and sequenced on a NextSeq500/550 (Illumina) instrument following recommended read configurations. BCL files were then converted to FASTQ files using bcl2fatstq (v2.15.1). Reads were filtered, aligned, and quantified using the 10X Cellranger computational suite (vX.3.1) to generate UMI-collapsed gene by cell count matrices.

scRNA-seq preprocessing of vitiligo scRNA-seq and scTCR-seq data. The Seurat (version 4.4.0) package was used to exclude low-quality barcodes, resulting in a total of 52,016 barcodes that met the following criteria: log10GenesPerUMI (complexity) exceeding 0.75; number of UMIs between 250 and 60,000; number of genes between 200 and 5,500; and mitochondrial reads less than 20%. Once these high-quality barcodes were obtained, non-PseudoY genes were removed from the dataset, resulting in a total of 20,688 genes analyzed across 52,016 cells from 10 donors. Subsequently, the Seurat package was employed to integrate the filtered gene-by-cell matrices, which were then analyzed using a typical unsupervised procedure including normalization, scaling, dimensionality reduction, batch correction, cell clustering, and differential gene expression analysis.

TCRs were called using CellRanger and filtered to a final set of 3,808, selected for overlap with scRNA-seq data and the presence of a single alpha and beta chain. Clonotypes were defined by V/J gene usage and CDR3 sequences of both chains. Only TCRs with paired transcriptomic data from quality-controlled cells were retained. scRNA-seq data included samples from both blister fluid and blood as annotated in the final scRNA-seq metadata; only TCRs from blister fluid were retained for analysis.

Determination of enriched variable gene segments in melanocyte-reactive TCRs. We used a Fisher's exact test to compute the enrichment of V alleles in melanocyte- or MART-1-reactive TCRs compared to all non-reactive TCRs or top undetected TCRs. Top undetected TCRs were defined as TCRs with clonal frequency greater than or equal to the top 25% cutoff of the 'others' distribution shown in Figure 5F.

Signature analyses with scRNA-seq data. To determine signatures of melanocyte-reactive and viral-reactive cells, differential expression analyses of antigen-reactive cells were performed comparing them against all other cells using MAST[88] with a covariate (latent_vars) for donor. Genes differentially expressed at FDR $P < 0.05$ and log-fold change > 0.58 (fold change 1.5) were carried forward for signature analyses. To compare our signatures to signatures from Lowery et al.[54] and Oliveira et al.,[7] the

Please cite this article in press as: Gaglione et al., Scalable TCR synthesis and screening enable antigen reactivity mapping in vitiligo, Immunity (2026), https://doi.org/10.1016/j.immuni.2026.01.001

AddModuleScore_Ucell() function was used in Seurat. Correlation analyses between signatures were restricted to cells harboring antigen-reactive TCRs in the indicated class (melanocyte-reactive or viral-reactive).

TCRdist analyses. We computed TCRdist with default parameters incorporating both germline segments and the amino acid sequence of the CDR3. For heatmap analyses in Figure S8, we downsampled the 'all others' class to 100 unique clones. For analyses examining the distribution of TCRdist (Figures S8C–S8F), all clones of the indicated classes were used, without downsampling.

Integration of vitiligo and melanoma scRNA-seq data. We obtained melanoma scRNA-seq data directly from the authors of Oliveira et al.[7] All T cell clusters were merged across the two datasets after stringent batch correction with Harmony,[89] adjusting for both donor and cohort. We used MAST with a covariate for donor to identify significantly differentially expressed genes between vitiligo melanocyte-reactive TCRs and melanoma neoantigen-reactive TCRs.

30,810 TCR library

Human paired TCR sequences were compiled from multiple sources including clinical trial NCT02305186,[66,67] and from whole blood and surgically resected tumor samples from patients with pancreatic ductal adenocarcinoma receiving treatment at Dana-Farber Cancer Institute (IRB #03-189 and #14-408). The study was conducted in accordance with the Declaration of Helsinki and the International Ethical Guidelines for Biomedical Research involving Human Subjects. Written informed consent was obtained from participants enrolled in #03-189 and #14-408 prior to sample collection.

For each PBMC sample, 6,000 cells were loaded into a 10X Chromium controller instrument along with Chromium Next GEM Single Cell 5' v2 beads (10X Genomics PN-1000263). Up to four PBMC samples were multiplexed together after being tagged with unique DNA-barcoded antibodies as described above. For tumor samples, all sorted cells were loaded, and no multiplexing was performed. After RT-PCR, cDNA was purified, and a library was constructed from each sample using a 10X Library Construction Kit (10X Genomics PN-1000190) following the standard 10X protocol. An additional VDJ-enriched library was created for each sample using a specialized Chromium Single Cell Human TCR Amplification Kit (PN-1000252). Libraries were then sequenced on an Illumina NovaSeq system operated by Azenta/Genewiz generating paired end 150bp reads.

The following steps were performed separately for each patient. First, the TCR contigs sequenced in the pre- and post-treatment sample were collapsed into one list to allow for clonotype assignment independent of time. The list was filtered to eliminate any non-productive rearrangements and sequences obtained from cells that did not pass QC, as described above. Then, a tentative clonotype was assigned to each unique combination of 1 to 4 TCR chains that co-occurred in one cell; a TCR chain was defined as the productive combination of a V gene, D gene (for β chains only), J gene, and complementarity determining region 3 (CDR3). Clonotypes were finalized by reassigning any cell if its TCR chain set formed a subset of another clonotype. A clonotype was considered to be shared between the blood and the tumor sample of a given patient if at least one match occurred in the α-chain or the β-chain CDR3 amino acid sequence.

Expression of TCRs in reporter Jurkat J76 cells

Jurkat J76 cells were lentivirally transduced to express CD8α and β chains in addition to a fluorescent reporter under the control of a nuclear factor of activated T cells (NFAT) response element.[39] Cells transduced by NFAT-CFP-encoding lentivirus were sorted as single cells into a 96-well plate and cultured until confluent. Half of each clonal population was stimulated with phorbol 12-myristate 13-acetate (PMA,10 ng/mL, Thermo Fisher) and ionomycin (1 ug/mL, Thermo Fisher). Reporter CFP expression was compared between stimulated cells and unstimulated cells and a clone with the highest differential was selected. The selected clone is henceforth referred to as NFAT-CFP $CD8^+$ J76.

TCR-encoding lentivirus was produced by transiently transfecting HEK293T cells with psPAX2 packaging plasmid and pMD2.G VSV envelope plasmid, and TCR library transfer plasmid at a ratio of 5.6:3:1 (per T225 flask: 22.5 μg psPAX2, 7.5 μg pMD2.VSVG, 42 μg TCR library transfer plasmid) in addition to TransIT-Lenti Transfection Reagent (Mirus Bio) at a 3:1 ratio of transfection reagent to DNA. Opti-MEM (Thermo Fisher), transfection reagent, and DNA were mixed and incubated for 10 minutes prior to dropwise addition to confluent HEK293T cells. Lentivirus was collected at 48 and 72 hours, centrifuged at 300*g* for 5 minutes to eliminate debris, and filtered through a 0.45-μm polyethersulfone filter (Millex, Millipore Sigma). Concentrated lentivirus (200×) was generated by ultracentrifugation at 100,000*g* for 90 minutes at 4C. Supernatant was discarded, and the pellet was resuspended overnight in 100 μL of Opti-MEM at 4C. Resuspended virus was aliquoted and stored at -80C.

Lentivirus was titered and NFAT-CFP $CD8^+$ J76 cells were transduced at an MOI of 0.05. Transduced cells were sorted on a BD FACSAria at a minimum coverage of 1000× for the 3,808 TCR library and 100× for the 30,810 TCR library to generate TCR library-expressing reporter J76 cells.

For individual clonal TCR lines, TCR constructs were formatted as TCRβ-P2A-TCRα and cloned into the same pHIV backbone vector as the TCR library. NFAT-CFP $CD8^+$ J76 cells were transduced with unconcentrated TCR lentivirus generated as described above (1 mL per 1M cells) and TCR expression was verified by flow cytometry with anti-TCR antibody (clone IP26, BioLegend).

Library-versus-library RAPTR lentiviral screening assay

Assembly of RAPTR 101-pMHC virus library

Lentivirus activated by promoter shuffling (LeAPS) virus libraries were produced as previously described in Dobson et al.[32] Briefly, HEK293T cells were seeded as described 24 hours pre-transfection. Libraries of 101 barcoded GFP-expressing pLeAPS plasmids and 101 pHIV-pMHC plasmids (GenScript) (Table S2) were used to generate VSVG-pseudotyped lentivirus in array in 24-well plates. Following virus collection at 48 hours, HEK293T cells were seeded at 20% confluency and transduced with pairs of barcoded LeAPS

and pMHC viruses in duplicate 24-well plates (per well: 100 μL barcoded LeAPS virus and 700 μL pMHC virus) with the addition of 8 μg/mL of diethylaminoethyl-dextran (Sigma-Aldrich) to aid transduction.

After 48 hours, duplicate wells were examined via flow cytometry for transduction by pMHC virus ($mCherry^+$) and LeAPS-barcode virus (GFP^+). The duplicate wells in culture were pooled proportionally according to the proportion of pMHC- and LeAPS barcode-transduced ($mCherry^+$ GFP^+) cells to ensure proportional representation of each pMHC library member. Pooled cells were sorted ($mCherry^+$ GFP^+) to generate the 101-pMHC virus-packaging cell line. To generate pMHC virus, virus-packaging cells were seeded analogously as HEK293T cells for transfection with psPAX2 and pMD2.VSVG-mut plasmids using *Trans*It-Lenti (Mirus Bio) transfection reagent. 101-pMHC virus library was collected and concentrated at 48 and 72 hours as described above.

RAPTR viral library stimulation

To stimulate the 3,808 TCR library with the 101-pMHC virus library, 65 million cells were incubated in complete RPMI with 560 μL of concentrated 101-pMHC virus library and 8 μg/mL of diethylaminoethyl-dextran (Sigma-Aldrich) for 24 h at 37C. Cells were washed once in FACS buffer and NFAT-CFP^+ cells were sorted on a BD FACSAria cell sorter.

RAPTR scRNA-seq of transduced cells

Prior to single-cell sequencing cells to extract TCRs enriched by stimulation with the 101-pMHC virus library, cells were sorted for transduction (GFP^+). Cells were analyzed using the 10x Genomics Chromium GEM-X Single Cell 5' v3 kit (PN-1000699). 0.5 μL of 10 μM custom TCR-specific primer (10X_TRAC_RT) was spiked into the reverse transcription (RT) mix to maximize TCR capture and a pMHC barcode-construct specific primer was added to the cDNA amplification mix (1 μL of 10 μM 10X_pMHC_cDNA) followed by a 0.65× SPRIselect bead (Beckman Coulter) cleanup. TCR amplicons were generated from cDNA via two nested PCRs: PCR #1 (98C for 45 sec; 15 cycles of 98C for 20 sec, 62C for 30 sec, 72C for 30 sec; 72C for 1 min) with 0.2 μM of 10X_nested_f and 10X_TCR_outer_r using KAPA HiFi HotStart ReadyMix (Roche) followed by a left-sided 0.8× SPRIselect bead cleanup; PCR #2 (98C for 45 sec; 13 cycles of 98C for 20 sec, 62C for 30 sec, 72C for 30 sec; 72C for 1 min) with 0.2 μM of 10X_nested_f and 10X_TCR_inner_r followed by a left-sided 0.8× SPRIselect bead cleanup. pMHC amplicons were generated from cDNA via PCR (98C for 45 sec; 25 cycles of 98C for 20 sec, 62C for 30 sec, 72C for 30 sec; 72C for 1 min) with 0.2 μM of 10X_nested_f and 10X_pMHC_r followed by a left-sided 0.8× SPRIselect bead cleanup. TCR and pMHC amplicons were indexed, pooled, and sequenced (150 bp PE) on an Element AVITI.

RAPTR scRNA-seq analysis

Cell-feature matrices were constructed for both TCR and pMHC amplicons using 10X CellRanger (v9.0.1). Unique 44-bp CDR3β barcodes were used as feature references to identify TCRs and 18-bp barcodes were used to identify pMHCs. Downstream analysis was completed in Python. In each dataset, cells with < 5 TCR or pMHC UMIs and cells with less than 60% of UMIs corresponding to a single TCR identity were filtered out. Each cell was assigned a TCR or pMHC identity based on the highest number of UMIs for each. The TCR and pMHC datasets were merged on cell barcodes, ensuring each cell had both a TCR and pMHC identity. TCR identities with fewer than 5 cells were filtered out. Plots were generated using Matplotlib and Seaborn packages.

Peptide-APC and J76 library co-culture screen

Peptides were selected from several sources for screening using antigen-presenting cells. The Immune Epitope Database (IEDB) was used to assemble a list of HLA-A2-binding human self-epitopes derived from genes that had been previously confirmed as generating immunogenic antigens in the context of vitiligo or melanoma. To identify novel candidate antigens specific to melanocytes, scRNA-seq data from melanocytes isolated from vitiligo donors were integrated with melanocyte scRNA-seq data from 17 donors profiled in Gellatly et al.[58] Genes specifically expressed in melanocytes were identified by performing differential expression analysis between melanocytes and all other cell types. Genes significantly upregulated (FDR-adjusted $P < 0.05$) and exhibiting a log-fold change > 1 were selected. This set was then intersected with melanocyte-specific gene lists derived from external datasets.

Melanocyte-specific gene expression in external datasets was identified using a multi-step data integration approach leveraging three datasets: the FANTOM5 project,[90] GTEx Portal,[91] and the single-cell analysis study by Belote et al.[92] In the FANTOM5 database, genes were selected if their expression was more than twofold higher than in any other tissue and exceeded 5 Transcripts Per Million (TPM) in the melanocyte categories of "Melanocyte.dark," "Melanocyte.light," or "Melanocyte." This yielded 227 candidate genes. Gene expression data from the GTEx Portal were then used to further refine the list to focus on skin-specific expression. Genes with higher expression in "Skin – Sun Exposed (Lower leg)" and "Skin – Not Sun Exposed (Suprapubic)" compared to all other non-brain and non-nerve tissues were prioritized, resulting in 13 genes with elevated expression in these skin tissues. Expression of proteins from these genes in melanocytes was then confirmed using a dataset from Belote et al.,[92] leading to the identification of five known melanocyte-specific genes: *PMEL, MLANA, TYRP1*, and *DCT*. Excluding these genes that have been extensively examined in vitiligo, 10 genes were selected for screening (*CD63, CDH3, CYGB, GMPR, GPR143, PLP1, SLC1A4, SOX10, VAT1*). Epitopes predicted to bind HLA-A2 were selected for screening using NetMHCpan version 4.1. Epitopes associated with extracted TCRs in VDJDb[68] were also included. We further assembled a list of melanoma-associated epitopes from literature.[44,46,47]

All peptides (GenScript) were pooled as described in Table S2 at 5 mg/mL in dimethyl sulfoxide. TAP-deficient T2 cells were pulsed with peptide pools at 10 μg/mL or individual peptides at 1 μg/mL for 4 h and incubated at a 1:1 ratio with TCR-expressing NFAT-CFP $CD8^+$ J76 cells at 37C for 20–24 h. Individual peptide validation was completed in 96-well U-bottom plates. Cells were washed and stained with anti-CD69 (Biolegend, clone FN50) and anti-CD19 (Biolegend, clone HIB19) in FACS buffer, both at a 1:200 dilution. Cells were analyzed for activation ($NFAT^+CD69^+$) on a Cytoflex S flow cytometer. For peptide pools, activated cells were sorted with a BD FACSAria cell sorter.

Please cite this article in press as: Gaglione et al., Scalable TCR synthesis and screening enable antigen reactivity mapping in vitiligo, Immunity (2026), https://doi.org/10.1016/j.immuni.2026.01.001

Bulk sequencing of TCRs enriched by antigen screens

To identify TCRs enriched by screens with the 101-pMHC virus library or peptide-pulsed T2 cells, genomic DNA was isolated from J76 cells using the PureLink Genomic DNA kit (Thermo Fisher). Noting that CDR3α and CDR3β were ordered on a single oligo and that each was codon-optimized to uniquely encode a specific TCR, extracting either CDR3α or CDR3β enabled identification of the full TCR clonotype. Using the CDR3β to identify TCRs in this assay, TRBV-CDR3β amplicons were amplified (98C for 30 sec; 24 cycles of 98C for 30 sec, 70C for 30 sec, 72C for 45 sec; 72C for 1 min) from 1 μg of genomic DNA using NEBNext Ultra II Q5 Master Mix (NEB) and 1 μM of each forward and reverse primer (for TCR: TRBV_CDR3B_f and TRBV_CDR3B_r; for pMHC: pMHC_BC_f and pMHC_BC_r). Amplicons were submitted for Amplicon-EZ analysis by Genewiz. Enrichment was calculated for each TCR as the fraction of reads for each enriched TCR divided by the TCR frequency in the base TCR library cell line quantified by sequencing on an Element AVITI (300 bp PE).

Individual functional TCR validation

Monoclonal TCR lines were established by assembling individual TCRs in pHIV backbones, generating unconcentrated TCR lentivirus as described above, and transducing 1 million NFAT-CFP $CD8^+$ J76 cells with 1 mL of unconcentrated virus, verifying expression by staining with anti-human TCR antibody (BioLegend, clone IP26). T2 cells were pulsed with individual peptides (Genscript) at 1 μg/mL for 2-4 hours. 100,000 peptide-pulsed T2 cells were incubated with 100,000 monoclonal TCR-expressing NFAT-CFP CD8 J76 cells overnight. Cells were washed and stained with anti-CD69 (Biolegend, clone FN50) and anti-CD19 (Biolegend, clone HIB19) in FACS buffer (PBS + 0.1% BSA + 1 mM EDTA) (1:200 dilution), before analysis on a Cytoflex S flow cytometer.

Antibodies in flow cytometry

All antibodies were used at a 1:50 or 1:200 dilution from stock concentration as described. Cells were stained in FACS buffer (PBS + 0.1% BSA + 1 mM EDTA) for 20 minutes at 4C, washed, and sorted on a BD FACSAria or analyzed on a Cytoflex S. All antibodies are from BioLegend.

QUANTIFICATION AND STATISTICAL ANALYSES

Statistical analyses were performed using Python or GraphPad Prism (v.10). Information on specific statistical tests is included in figure legends. Data in bar plots is represented as the mean ± S.D. as indicated in figure legends. *P* values are listed in figure legends.

Software

Graphs were generated using Python and GraphPad Prism (v.10). Flow cytometry data were analyzed by FlowJo (v.10.10.0).